Influence of Matrix Strength
on Pullout Behavior of Bundled Aramid Fiber in FRCC

WANG JIN
(Master's Program in Engineering Mechanics and Energy)

Advised by Toshiyuki Kanakubo

Submitted to the Graduate School
of Science and Technology Degree Programs
in Systems and Information Engineering
in Partial Fulfillment of the Requirements
for the Degree of Master of Engineering
at the
University of Tsukuba

March 2022

Abstract

Fiber-reinforced cementitious composite (FRCC) is a cementitious material mixed with short discrete fibers, which shows good ductile behavior under tensile and bending stress. The bridging law, i.e., the tensile stress-crack width relationship has been proposed to evaluate the performance of the FRCC in recent years. For practical applications, an effective and accurate method of the constitution of the bridging law is pursued eagerly. As the essential part of the constitution of the bridging law, a precise and practical evaluation method for the single-fiber pullout test is also indispensable.

This study evaluates the influence on the matrix strength in a pullout test of bundled aramid fibers. The modification of bundling shows an unsmooth surface for aramid fibers which is expected to exhibit an excellent bonding to the cementitious matrix. For the cementitious matrix, the improvement of the matrix strength, i.e., the reduction of the water/cement ratio means better densification of the cementitious materials, is considered to provide a superior interface property to exert better bonding stress for the bundled aramid fiber.

The pullout test of bundled aramid fibers was carried out considering various parameters, including the matrix strength, the embedded length, and the inclined angle of the fiber. The influences of matrix strength in different embedded lengths and inclined angles were evaluated based on the result of the pullout test. A power function relationship was found between the maximum pullout load and the embedded length. The subbing effect, which describes the influence of inclined angle, is also observed.

Based on the test result, a bilinear model was established to describe the single fiber's pullout behavior. A group of empirical formulas, in which the maximum pullout load, effect of embedded length, and snubbing effect were expressed as the functions of matrix strength, were proposed based on the test results. From the calculation result of bridging law, the maximum tensile stress increases almost proportionally as the matrix strength becomes larger.

Influence of Matrix Strength on
Pullout Behavior of Bundled Aramid Fiber in FRCC

CONTENTS

List of Figures

List of Tables

Chapter 1 Introduction

1.1 Research Background

Traditional concrete shows good performance under compressive stress. However, such material usually fails by the unstable propagation of the crack under tensile stress. Recently, a brand-new material called Fiber Reinforced Cementitious Composites (FRCCs) has been proposed. FRCC is a cementitious material mixed with discrete short fibers into cementitious matrix. With the reinforcement effect of short fibers, FRCC performs a good strength, ductility, and toughness under tensile stress. As shown in **Fig. 1.1**, after the first crack of the matrix, short fibers bridging the crack sustain uniaxial tension by the bridging effect. Individual fibers existing at the matrix crack surface play an essential role in suppressing the further growth of the crack

In the past several decades, many types of FRCCs have been studied, such as engineered cementitious composite (ECC), strain hardening cement composite (SHCC), and ductile fiber-reinforced cementitious composite (DFRCC). ECC and SHCC show strain hardening and multiple fine crack behavior under uniaxial tension. DFRCC is defined as a type of FRCC showing deflection hardening and multiple cracks under bending conditions.

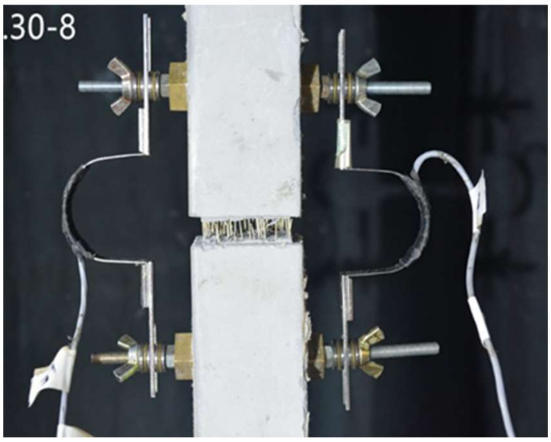

Fig. 1.1. FRCC under uniaxial tensile stress [1]

1.2 Pullout Behavior of Single Fiber

1.2.1 Pullout Test

To predict and evaluate the behavior of the fiber-bridging effect, a calculation model called bridging law [2] has been proposed. The bridging law is explained as a tensile stress-crack width relationship that characterizes tensile performance after the first cracking of the matrix. The bridging law can be obtained by an integral calculus of forces carried by individual fibers bridging the crack, considering the probability density function for the fiber inclined angle and distribution.

As shown in **Fig. 1.2**, with the evaluation of the single fiber pullout behavior, it is possible to predict the actual behavior of structural elements by the constitution method of the bridging law. Thus, the pullout behavior of a single fiber occupies an essential part of establishing the prediction model for applications. An accurate and practical method of the single fiber pullout test is needed eagerly.

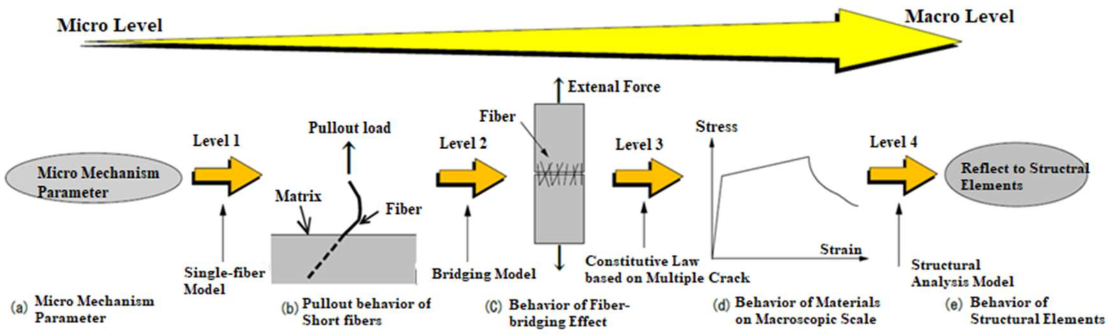

Fig. 1.2 The flow diagram of materials design [3]

Usually, a pullout test for the single fiber with a fiber's diameter less than 100μm is not easy because of the difficulty of the specimen's fabrication and the loading method. Although, many creative experiments were conducted to investigate the behavior of these thin fibers in the past several decades. Chan and Li [4] conducted the pull-out test for single steel, brass (both of 1.02mm diameter), and polyethylene fibers (two types: 38μm and 20μm) in different water cement ratio (W/C). They claimed that adhesive bond failure occurs in the steel-cement and polyethylene-cement boundaries, and cohesive bond failure occurs between brass and cement. They also suggested that the modification of the fiber surface would be necessary to enhance the adhesion between the fibers and the cement matrix. Li et al. [5] found that the force and energy at fiber pulling-out increase with the inclination angle of fiber by a pullout test for nylon and polypropylene fiber with a diameter of 508μm. They also offered an explanatory theory to predict the snubbing effect. Kanda and Li [6] concluded that PVA fiber has a high chemical bond and frictional bond strength by pulling out a single PVA fiber with a diameter of 14μm. They also found that the apparent strength of fiber decreases as the angle of inclination of the fiber increases. A practical function was proposed to express the degradation of the fiber strength. Kiyota et al. [7] conducted a group of pullout tests for single aramid, PVA, and PE fibers with diameters of 12μm, 37μm, 12μm, respectively. Different behaviors of the three types of fibers were clearly observed from the tests result. Curosu et.al. [8] reported differences in fiber-failure stress and bond strength in pullout test of HDPE, aramid, and PBO fibers with diameters of 20μm, 12μm, and 13μm, respectively.

1.2.2 Pullout Behavior

(1) Micromechanical model for interpretation of interface properties

Fiber-matrix interface properties can be explained as two parts: the debonding process and the pulling-out process. [6] **Fig. 1.3** shows a typical load-displacement relationship for the single fiber which has a better chemical than the frictional bond. In the debonding process, the chemical bond is broken gradually, and replaced by the constant frictional bond. An assumed shear-stress distribution near the debonding tip is shown in **Fig. 1.4**. When the shear stress overcomes a critical value τ_s, the interface property is substituted by a constant frictional bond τ_i. In other words, the bonding property of the pullout test for a single fiber can be interrupted by the chemical bond τ_s, and frictional bond τ_i.

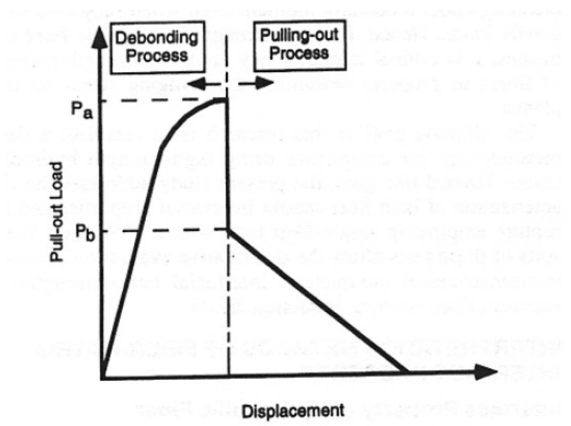

Fig. 1.3 Schematic of load-displacement relation for fiber pullout behavior [6]

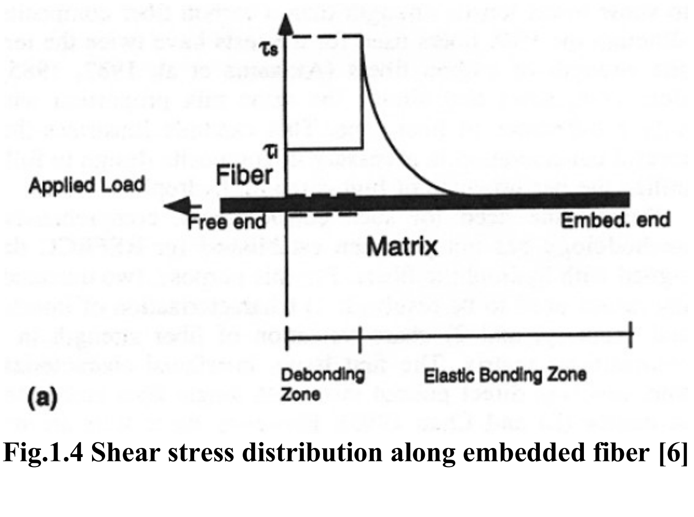

Fig.1.4 Shear stress distribution along embedded fiber [6]

Aramid fiber is known as one type of polymeric fiber with high tensile strength. Commercially provided aramid fibers have a diameter of 12μm, and a bundled aramid fiber made from several yarns usually has a diameter of 0.5mm. As for aramid fibers, a good chemical bond cannot be expected in the debonding process [7]. However, a bundled aramid fiber is expected to have an excellent mechanical bond because of its unsmooth surface. Thus, in the process of debonding, the mechanical resistance is dominant for the pullout behavior of bundled aramid fibers. Additionally, reducing the water/cement(W/C) ratio or using of silica fume can improve the matrix's densification around the fiber, enhancing the fiber-cement interfacial bond strength. [4]

(2) Influence of inclined angle

As Li et al. [5] pointed out that the snubbing effect influences the pullout behavior with a single fiber, that is the pullout load increases with the increase of inclined angle. As shown in **Fig. 1.5**, while the fiber is under the pullout force *P* with an angle *Φ*, the matrix wedge at the exit point of fiber exerts a normal force *N* to the fiber. Therefore, a friction force *F* is generated at the perpendicular direction of the force *N*. The pullout load *P* becomes more significant when the fiber is set at an angle. This is due to the resistance of the frictional force *F*.

The snubbing effect can be evaluated with Eq.(1.1).

$$P = P_0 \cdot e^{f \cdot \theta} \tag{1.1}$$

Where:

P: pullout load

P_0: pullout load at inclined angle 0

f: coefficient of the snubbing effect

θ: inclined angle of fiber

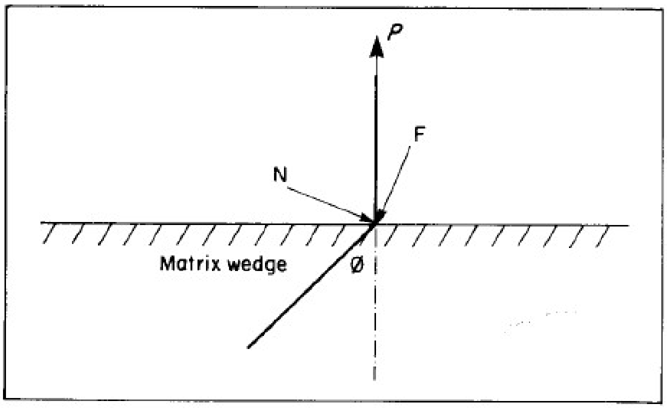

Fig. 1.5 Illustration of fiber pullout at angle [5]

Fig. 1.6 shows the experiment result for the snubbing effect. From the test results of nylon("+") and PVA("□") fibers, the pullout load increases as the inclined angle increases.

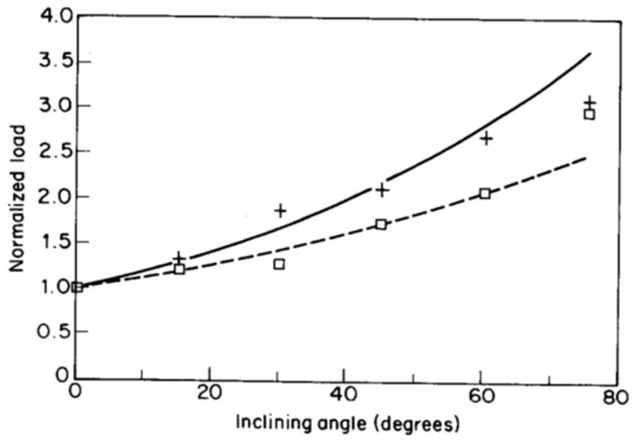

Fig. 1.6 The influence of inclined angle on the pullout load [5]

(3) Fiber ruptures

If the fiber's embedded length is long enough or the bond strength at the exit point of fiber is strong enough, a fiber rupture may occur when the fiber's strength is exceeded by the pullout load. This strength is usually less than the measured value of fiber strength provided by the manufacturers. When the fiber is aligned obliquely, additional stress is induced by bending at the exit point of the fiber-matrix interface. This apparent strength of fiber decreases as the inclined angle of the fiber becomes larger, and Eq.(1.2) proposed by Kanda. and Li. [6] expresses the degradation effect of the apparent fiber strength.

$$\sigma_{fu} = \sigma_{fu}^{n} \cdot e^{-f' \cdot \phi} \tag{1.2}$$

Where:

σ_{fu}: apparent strength of fiber

σ_{fu}^{n}: rupture strength of fiber at angle $\phi = 0$

f': apparent fiber strength reduction factor

1.3 Research Objective

The main objective of this study is to evaluate the influence of matrix strength on the pullout behavior of bundled aramid fiber. To achieve the research goal, pullout test is conducted for bundled aramid fiber in three different matrix strengths to accurately model. The bridging law is constructed based on the test results of the pullout test to evaluate the influence on the matrix strength.

Chapter 2 Experiment Outline

2.1 Used Materials

The mixture proportion of the cementitious matrix is shown in **Table 2.1**. The proportion is designed based on the previous study[9]. The water-to-binder ratio is controlled invariantly to ensure the constant flowability of the matrix. To obtain different matrix strength, the water-cement ratio (W/C) is changed to 0.785, 0.560, and 0.436. Portland cement of high early strength is used to ensure that the target matrix strength is achieved in the early phase of curing.

Aramid bundled fibers are used, as shown in **Fig. 2.1**. The bundled aramid fiber is a bundle of aramid yarns with a nominal diameter of 12μm. The original yarns are twisted to form a single thick

Table 2.1 Mixture proportion of cementitious matrix

Target matrix strength	Water by Cement ration	Water by Binder ratio	Flyash by Binder ratio	Unit Weight(kg/m^3)			
				Water	Cement	Fly ash	Sand
Fc24	0.785	0.392	0.500	380	484	484	484
Fc36	0.560	0.392	0.300	380	678	291	484
Fc48	0.436	0.392	0.100	380	872	97	484

Cement: High early strength Portland cement
Fly ash: Type Ⅱ of Japanese Industrial Standard (JIS A 6206)
Sand: Size under 0.2mm
High-range warter-reducing admixture: Binder × 0.6%

(a) **(b)**
Fig. 2.1 Aramid fibers used in this study:
(a)Bundled fibers; (b)Appearance of yarns.

Table 2.2 Physical property of aramid fibers

Type of the fiber	Diameter (mm)	Tensile strength* (MPa)	Elastic modulus* (GPa)
Aramid	0.5	3432	72

*Measured value before bundling

fiber and sized not to unravel in the FRCC. The physical property before bundling of aramid fiber provided by manufacturers is shown in **Table 2.2**.

For the purpose of investigating compressive strength of FRCC with aramid bundled fiber, uniaxial compression test was conducted. Chopped aramid bundled fibers with a length of 30mm are used. The volume fraction of fibers is set to 1% (unit weight: 13.9kg/m^3) and 2% (unit weight: 27.8kg/m^3).

As shown in **Fig. 2.2**, a universal testing machine with a loading capacity of 500kN is used in the test. The test piece was made with a cylinder mold with a diameter of 100mm and a height of 200mm. To reduce the scattering of the test result, three specimens were cast for each mixture proportion. Also, a fiber-free control group is manufactured for each test series.

Fig. 2.2 Loading method of uniaxial compression test

2.2 Pullout Test for Single Aramid Fiber

2.2.1 Specimens

Continuous aramid fiber before cutting is used for pullout test. Details of mold fabrication are shown in **Fig. 2.3**. The pullout test specimen is a square plate with a size of 30mm×30mm. The single fiber is embedded in the center of the plate. The mold is made by two acrylic plates and three rubber plates, as shown in **Fig. 2.3(b)**, a total of five plates are fixed by bolts at four corners. The thickness of the specimen is equal to the embedded length of the fiber. It is controlled by the thickness of the middle rubber plate. A tiny hole is opened in the center of the acrylic plate and rubber plates to fix the single fiber in the perpendicular direction. As shown in **Fig. 2.3(c)**, the injection hole is designed for casting, while the ventilator hole is used to avoid the generation of air void in the matrix.

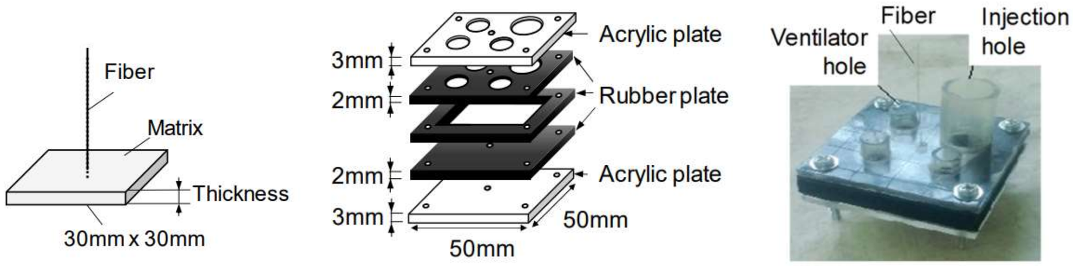

(a) (b) (c)

Fig. 2.3 Pullout specimen: (a) Dimensions of pullout specimen; (b) Constitute of mold; (c) Example of mold.

The test parameters are the strength of matrix, the embedded length of fibers, and the inclined angle of fibers. **Table 2.3** shows details of specimen for the pullout test. Five replicate specimens are manufactured for each parameter to reduce the scattering of the test results. The series of specimens is designated by its matrix strength, the embedded length of fibers, and the inclined angle of fibers. For example, the designation of "Fc36-8mm-30" represents the specimen with a matrix strength of Fc36, embedded length of 8mm, and inclined angle of 30°. The fiber length out of the matrix is fixed at 55mm to control the deformation of the fiber, which will be discussed later.

Table 2.3 List of specimens for the pullout test:(a) Matrix strength of Fc24, (b)Matrix strength of Fc36, (c)Matrix strength of Fc48.

(a):

Specimen Designation	Designed embedded length (mm)	Incilned angle (°)	Fiber length out of the matrix (mm)
FC24-4mm-0	4	0	55
FC24-4mm-15		15	55
FC24-4mm-30		30	55
FC24-4mm-45		45	55
FC24-4mm-60		60	55
FC24-8mm-0	8	0	55
FC24-8mm-15		15	55
FC24-8mm-30		30	55
FC24-8mm-45		45	55
FC24-8mm-60		60	55
FC24-12mm-0	12	0	55
FC24-12mm-15		15	55
FC24-12mm-30		30	55
FC24-12mm-45		45	55
FC24-12mm-60		60	55

(b):

Specimen Designation	Designed embedded length (mm)	Incilned angle (°)	Fiber length out of the matrix (mm)
FC36-4mm-0	4	0	55
FC36-4mm-15		15	55
FC36-4mm-30		30	55
FC36-4mm-45		45	55
FC36-4mm-60		60	55
FC36-8mm-0	8	0	55
FC36-8mm-15		15	55
FC36-8mm-30		30	55
FC36-8mm-45		45	55
FC36-8mm-60		60	55
FC36-12mm-0	12	0	55
FC36-12mm-15		15	55
FC36-12mm-30		30	55
FC36-12mm-45		45	55
FC36-12mm-60		60	55

(c):

Specimen Designation	Designed embedded length (mm)	Incilned angle (°)	Fiber length out of the matrix (mm)
FC48-4mm-0	4	0	55
FC48-4mm-15		15	55
FC48-4mm-30		30	55
FC48-4mm-45		45	55
FC48-4mm-60		60	55
FC48-8mm-0	8	0	55
FC48-8mm-15		15	55
FC48-8mm-30		30	55
FC48-8mm-45		45	55
FC48-8mm-60		60	55
FC48-12mm-0	12	0	55
FC48-12mm-15		15	55
FC48-12mm-30		30	55
FC48-12mm-45		45	55
FC48-12mm-60		60	55

2.2.2 Loading Method

Fig. 2.4 shows the schematic diagram for the loading method of the pullout test. A monotonic pullout load is applied using an electronic system universal testing machine with a capacity of 200N (LSC-02/30-2, Tokyo Testing Machine Co., Ltd., Tokyo Japan). The specimen is fixed via adhering to a steel plate. The inclined angle is set by tilting the steel plate as shown in **Fig. 2.4(b)**. The fiber is clamped by the chucking jig directly. The length of fiber out of the matrix is set to 55mm. The head speed is set to 1mm per minute. The pullout load and head displacement are recorded.

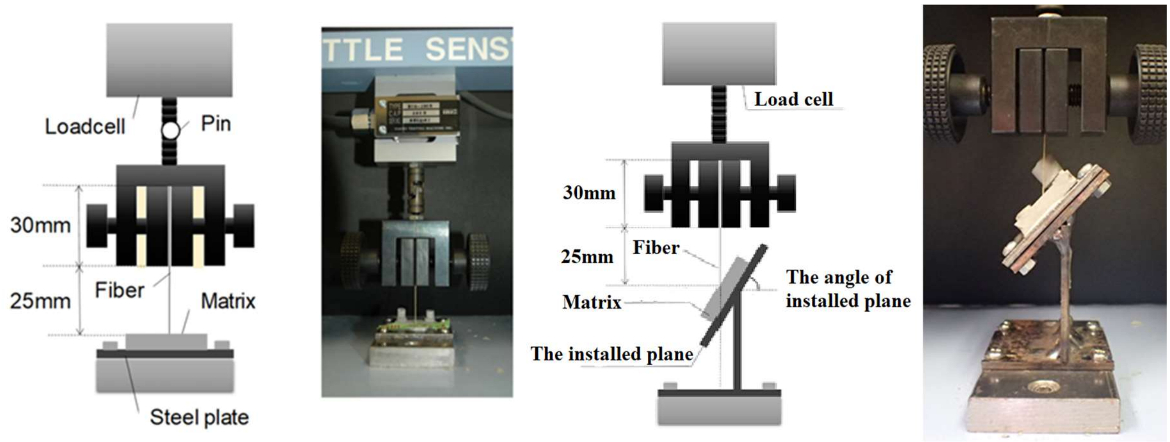

(a) **(b)**

Fig. 2.4 Loading method of pullout test:
(a)Specimen at inclined angle 0, (b)Specimen with inclined angle

2.2.3 Uniaxial Tension Test for Single Bundled Aramid Fiber

In the pullout test for the single fiber, the elongation of the fiber out of the matrix increases under a pullout load. This deformation of fiber is not expected to be included in record of slip.

The result of the uniaxial tension test is acquired from a previous study [9] that used identical type of fibers. As shown in **Fig. 2.5**, the fiber is directly grasped by the chunk jig at both ends. The fiber length out of the matrix is set to 55mm=30mm+25mm. From the test result, an approximate expression of the relationship between deformation and load was obtained as shown in Eq.(2.1). The slip of fibers s can be obtained using Eq.(2.2)

$$\delta = 7.43 \times 10^{-8}P^3 + 1.16 \times 10^{-6}P^2 + 0.0913P \tag{2.1}$$

$$s = x - \delta/2 \tag{2.2}$$

Where,

P: pullout load

s: slip of fiber

x: recorded head displacement

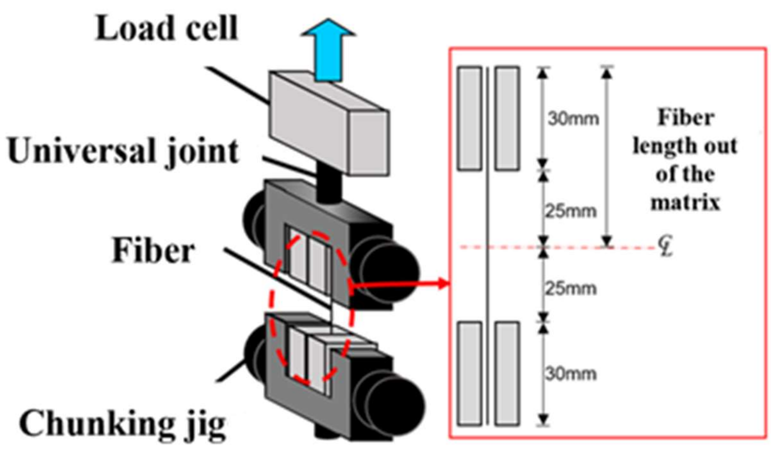

Fig. 2.5 Loading method of uniaxial tension test for single fiber

Chapter 3 Results of Experiment

3.1 Results of Uniaxial Compression Test

Table 3.1 shows the results of the uniaxial compression test. The test specimen is designated by its target matrix strength and the fiber volume fraction. For example, the specimen designation of "Fc36-1-1" represents the specimen with a target matrix strength of Fc36 and is mixed with fibers of 1% volume. The maximum load of the test piece is recorded, and the compressive strength is calculated by dividing the cross-sectional area of the cylinder specimen. Also, the young's modulus is calculated based on the relationship of stress-strain. A total of three specimens for each test series are tested and the average value is calculated.

On average, the compressive strength is in good agreement with the target matrix strength. It is apparent from this table that the compressive strength and young's modulus are not significantly influenced by fibers. This reveals that the addition of fibers has little effect on the compressive strength and young's modulus. The same property of FRCCs was also found in other studies [10][11].

Table 3.1 Results of uniaxial compression test:
(a)Matrix strength of Fc24, (b)Matrix strength of Fc36, (c)Matrix strength of Fc48.

(a):

Specimens Designation	Weight (kg)	Height (mm)	Diameter (mm)	Maximum load (kN)	Compressive strength (MPa)	Young's modulus (GPa)
Fc24-N-1	2947.9	197.4	100.0	212	27.0	11.0
Fc24-N-2	2978.4	198.7	100.0	205	26.1	11.6
Fc24-N-3	2954.4	198.7	99.2	207	26.4	10.9
Average	2960.2	198.3	99.7	208	26.5	11.2
Fc24-1-1	2909.8	198.6	99.8	196	24.9	11.3
Fc24-1-2	2918.6	199.0	99.8	189	24.1	10.9
Fc24-1-3	2910.4	197.3	100.0	190	24.2	11.4
Average	2912.9	198.3	99.8	192	24.4	11.2
Fc24-2-1	2929.7	198.7	100.5	189	24.1	11.2
Fc24-2-2	2926.8	198.8	100.2	190	24.2	10.5
Fc24-2-3	2941.3	199.4	100.0	185	23.6	10.4
Average	2932.6	199.0	100.2	188	24.0	10.7

(b):

Specimens Designation	Weight (kg)	Height (mm)	Diameter (mm)	Maximum load (kN)	Compressive strength (MPa)	Young's modulus (GPa)
Fc36-N-1	3020.7	197.3	100.1	297	37.8	14.8
Fc36-N-2	3025.2	198.6	100.2	278	35.4	15.1
Fc36-N-3	3019.3	199.1	100.0	300	38.2	14.9
Average	3021.7	198.3	100.1	292	37.1	14.9
Fc36-1-1	2998.2	198.6	100.4	275	35.0	15.2
Fc36-1-2	3013.8	199.1	100.3	249	31.7	15.3
Fc36-1-3	2993.0	197.9	100.4	296	37.7	15.1
Average	3001.7	198.5	100.3	273	34.8	15.2
Fc48-2-1	3051.5	198.1	100.3	283	36.0	14.5
Fc48-2-2	3031.1	196.9	100.2	276	35.1	14.3
Fc48-2-3	3002.8	195.3	100.4	268	34.1	14.7
Average	3028.5	196.8	100.3	276	35.1	14.5

(c):

Specimens Designation	Weight (kg)	Height (mm)	Diameter (mm)	Maximum load (kN)	Compressive strength (MPa)	Young's modulus (GPa)
Fc48-N-1	3083.6	198.5	100.0	430	54.7	17.0
Fc48-N-2	3076.1	197.6	100.1	412	52.5	17.2
Fc48-N-3	3099.1	199.0	100.0	397	50.5	17.9
Average	3086.3	198.4	100.0	413	52.6	17.4
Fc48-1-1	3026.6	196.5	100.2	409	52.1	16.3
Fc48-1-2	3068.0	198.7	99.9	422	53.7	18.3
Fc48-1-3	3071.3	198.4	100.0	434	55.3	18.7
Average	3055.3	197.9	100.0	422	53.7	17.8
Fc48-2-1	3062.1	200.6	100.1	409	52.1	17.1
Fc48-2-2	2999.8	196.9	100.0	407	51.8	17.1
Fc48-2-3	3043.8	198.0	100.0	432	55.0	16.9
Average	3035.2	198.5	100.0	416	53.0	17.0

3.2 Results of Pullout Test

3.2.1 Failure Details

In most specimens, as shown in **Fig 3.1**, the fiber is pulled out slowly from the matrix, and a tiny hole remains. The loading is finished simultaneously when all fiber parts are pulled out from the matrix. No damage on the matrix surface or any cracks around fiber is observed.

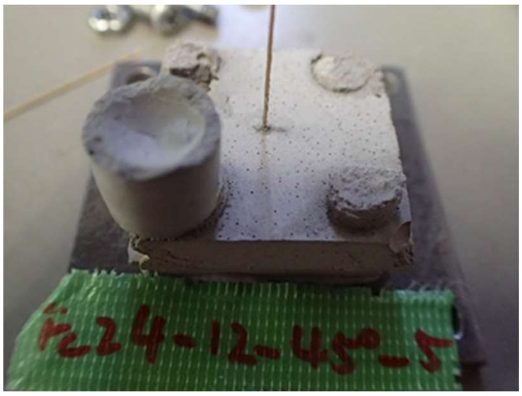

(a)

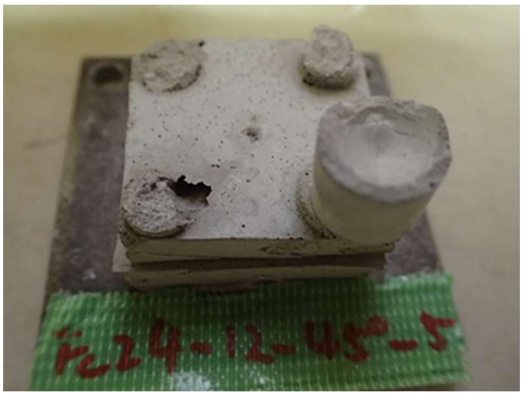

(b)

Fig. 3.1 Example of specimens:
(Matrix strength of Fc24, embedded length of 12mm, inclined angle at 45°)
(a)Before loading, (b)After loading

Fig. 3.2 shows the fiber condition after loading by a sequence of inclined angle from 0° to 60°. From this figure, apparent damage is observed around the embedded part of the fiber. Yarns at the embedded part of the fiber are unraveled after loading. This phenomenon appears more obviously in the specimen with a higher matrix strength and a larger inclined angle.

For the bundled aramid fiber, the mechanical force is predominant in the process of pulling out. In the process of pulling out, the surface of the fiber is damaged due to the matrix uneven surface. A stronger matrix brings deeper damage of the fiber. In addition, a large inclined angle may also intensify the force on the fiber owing to the snubbing effect. Thus, the phenomenon of unraveling is found more commonly in the case of higher matrix strength or a larger inclined angle.

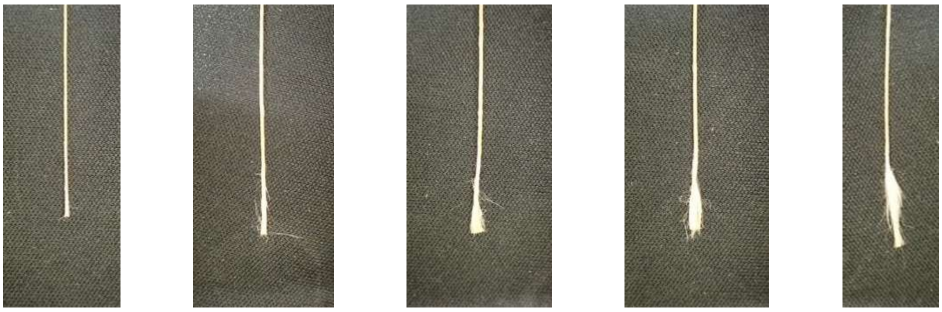

0° 15° 30° 45° 60°

Fig. 3.2 Example for the condition of fiber after loading
(Matrix strength of Fc48, Embedded length of 12mm)

In some specimens with long embedded lengths and large inclined angles, the fibers ruptured during the loading process. **Fig 3.3** shows an example of fiber rupture point. Previous study also showed this phenomenon in cases with a long embedded length and a large inclined angle(30°, 45°, 60°). No significant differences are found among different matrix strengths.

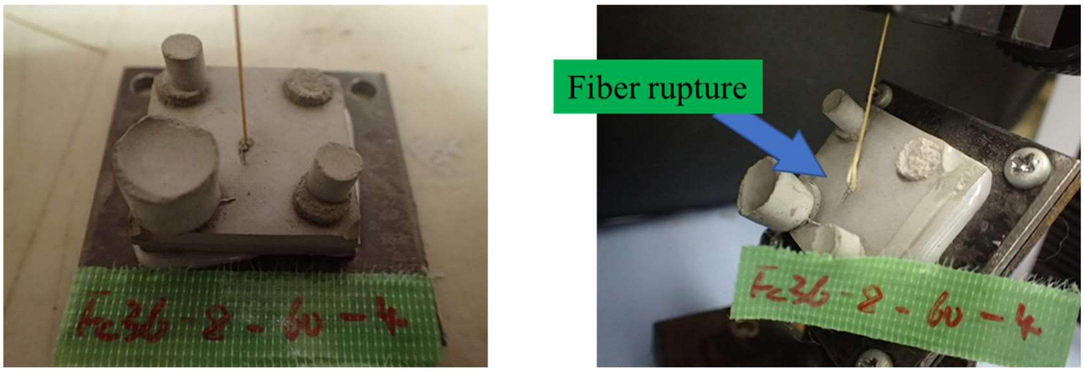

(a) (b)

Fig. 3.3 Example of fiber rupture:
(Matrix strength of Fc48, Embedded length of 8mm, inclined angle at 60°)
(a)Before loading, (b)After loading

3.2.2 Pullout Load-Slip Curves

Fig. 3.4 to **Fig. 3.12** show the relationship of pullout load-slip. The fiber deformation described in Chapter 2.2.4 is considered. Some specimens with crack before loading are excluded. At least four specimens are loaded for each series of tests. The average curve is calculated for each test series by linear interpolation. The specimens with ruptured of fibers, are not considered in averaging. The mark of "○" in each curve represents the maximum pullout load.

As shown from **Fig. 3.4** to **Fig. 3.12**, the curves generally show two stages. Before the maximum pullout load, the load increases linearly, then decreases slowly after the maximum pullout load. The pullout load becomes nearly null when the slip has reached the embedded length of fiber.

In some cases of matrix strength Fc24 with embedded lengths of 8mm and 12mm, the load decreases before reaching the embedded length. For example, as shown in **Fig. 3.5(a)** and **Fig. 3.6(a)**, the pullout load sustains a low value after the maximum pullout load until it is pullout out entirely. This property is not observed in the test series of matrix strength Fc36 and Fc48. Compared to the cases with embedded length of 4mm, as shown in **Fig 3.4**, it is considered that the matrix around the fiber is damaged in the debonding process due to the unsmooth surface of the bundled aramid fibers, which cannot provide enough resistance for the remaining part of the fiber. In other words, for bundled aramid fibers, enough bonding stress cannot be expected along the overall length of fibers with low matrix strength.

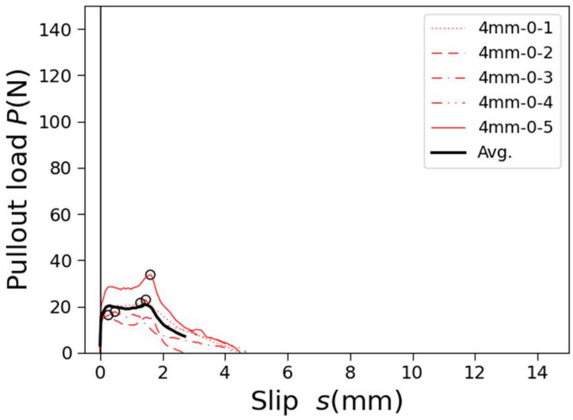

(a)

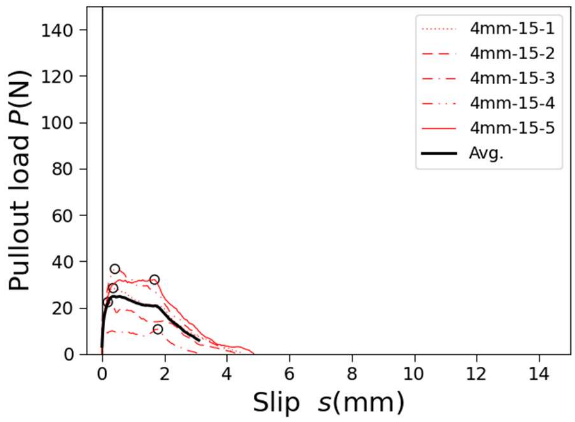

(b)

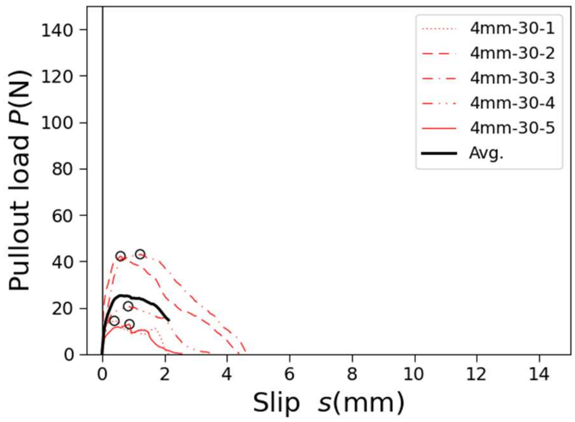

(c)

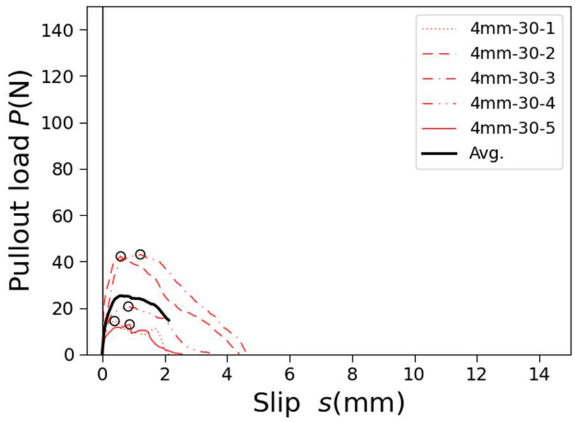

(d)

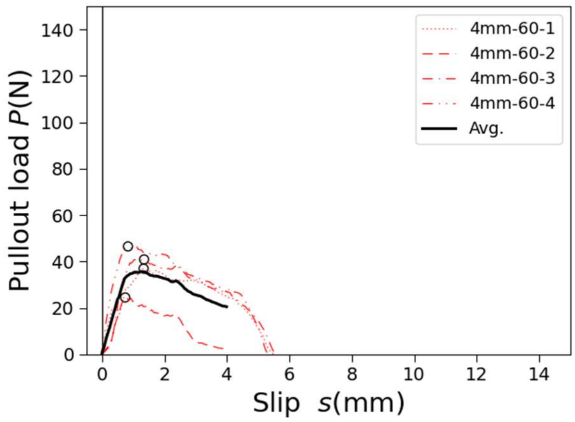

(e)

Fig. 3.4 Pullout load-slip relationship:
(Matrix strength of Fc24, Embedded length of 4mm)
(a)Inclined angle 0°, (b) Inclined angle 15°, (c) Inclined angle 30°,
(d) Inclined angle 45°, (e) Inclined angle 60°

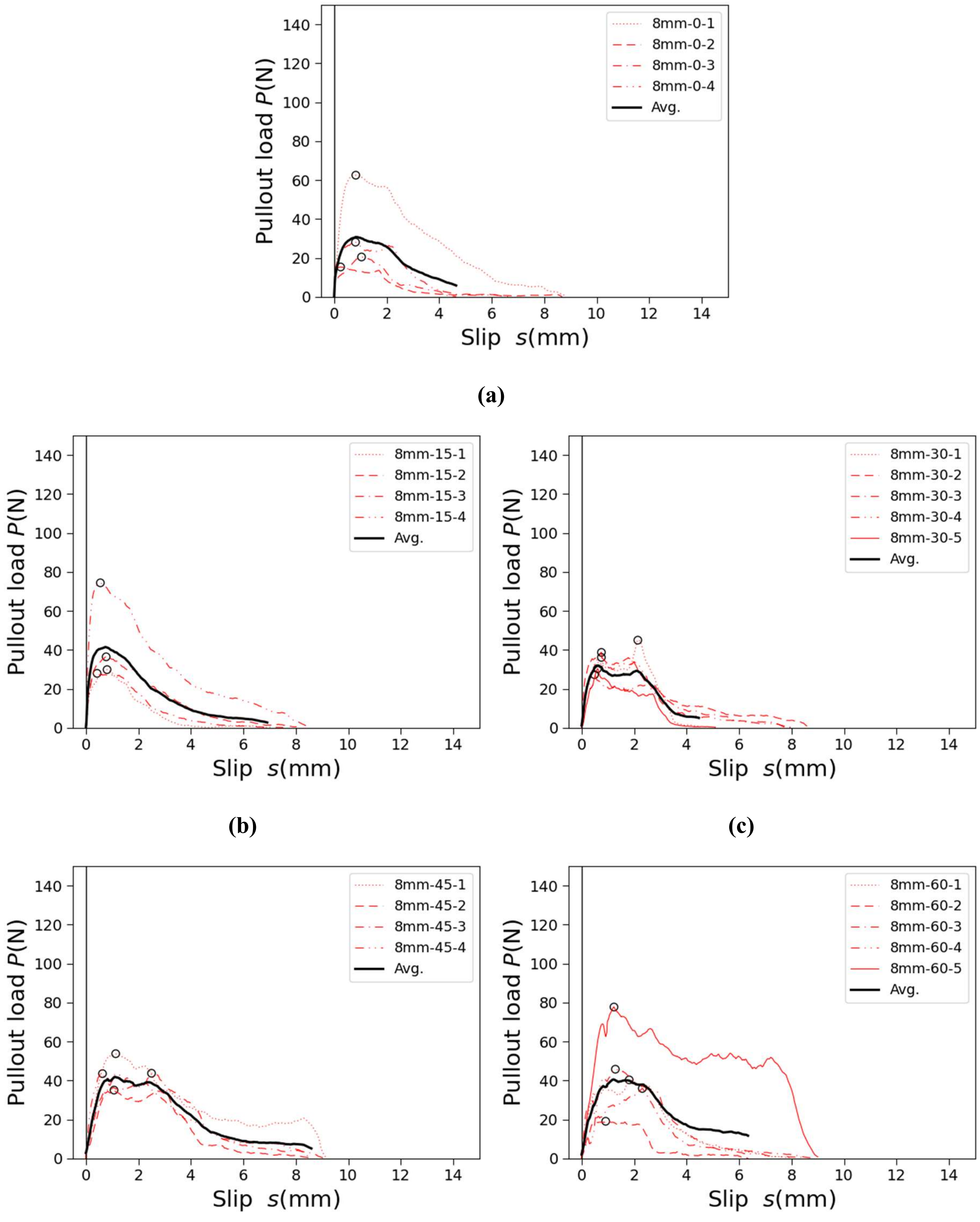

(a)

(b) **(c)**

(d) **(e)**

Fig. 3.5 Pullout load-slip relationship:
(Matrix strength of Fc24, Embedded length of 8mm)
(a)Inclined angle 0°, (b) Inclined angle 15°, (c) Inclined angle 30°,
(d) Inclined angle 45°, (e) Inclined angle 60°

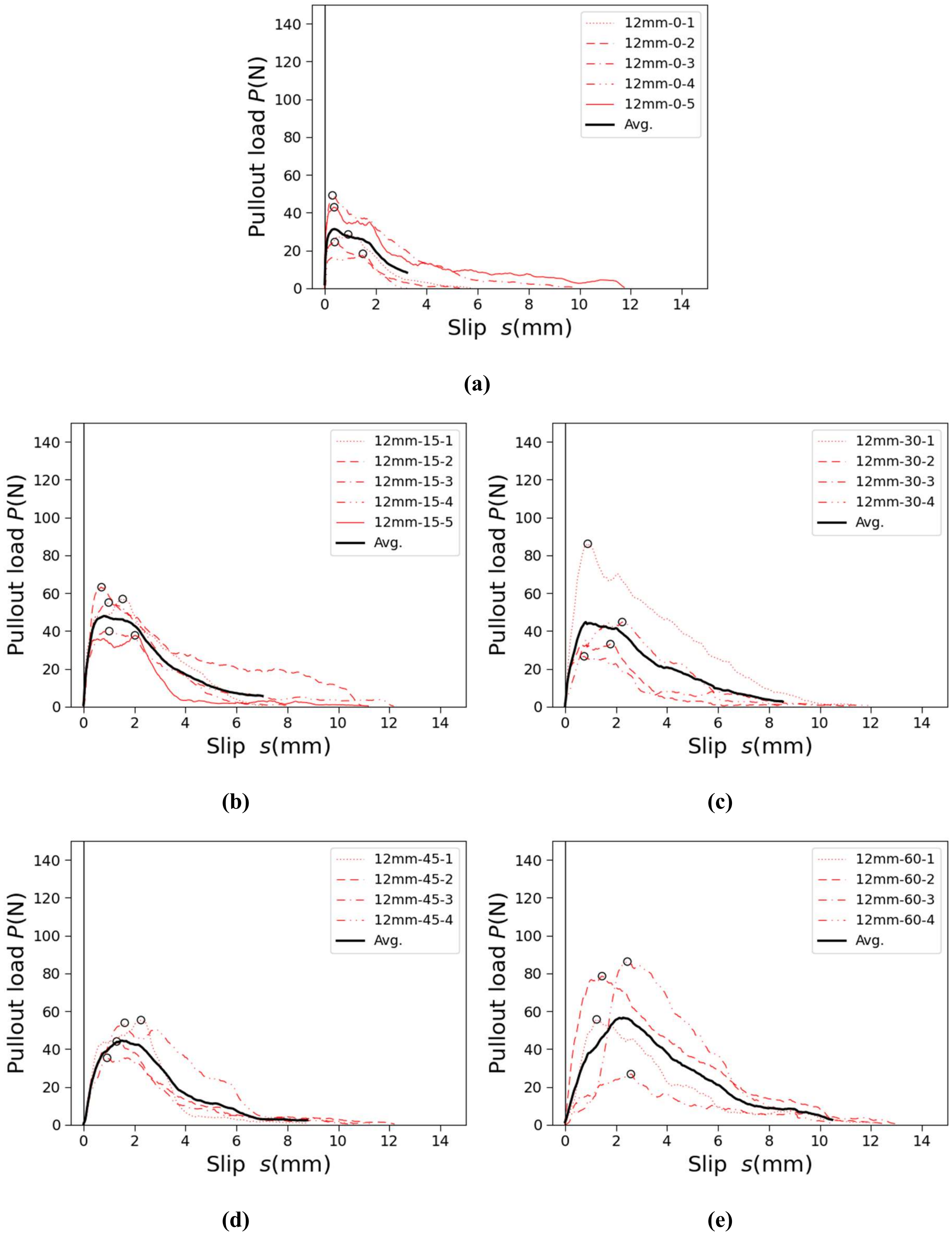

Fig. 3.6 Pullout load-slip relationship:
(Matrix strength of Fc24, Embedded length of 12mm)
(a)Inclined angle 0°, (b) Inclined angle 15°, (c) Inclined angle 30°,
(d) Inclined angle 45°, (e) Inclined angle 60°

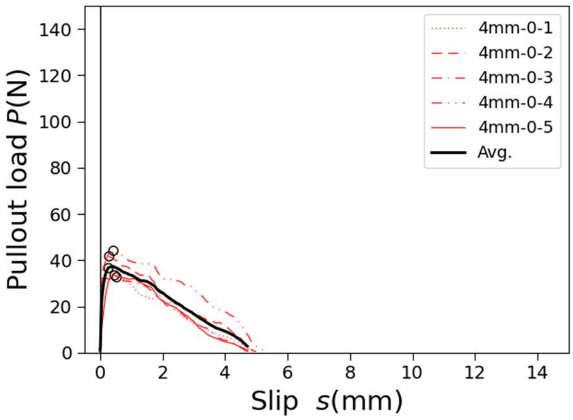

(a)

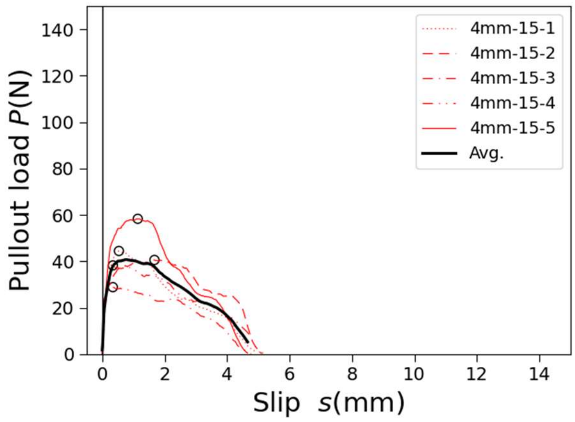

(b)

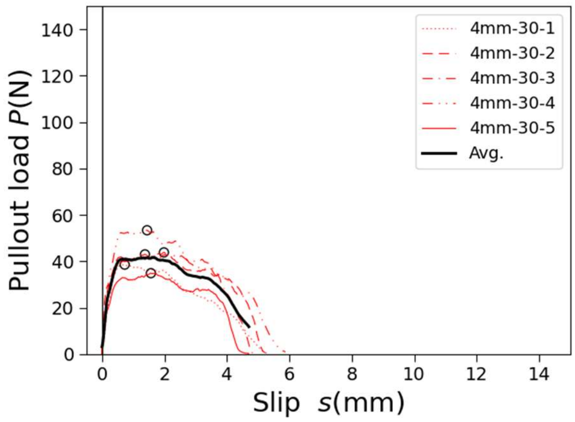

(c)

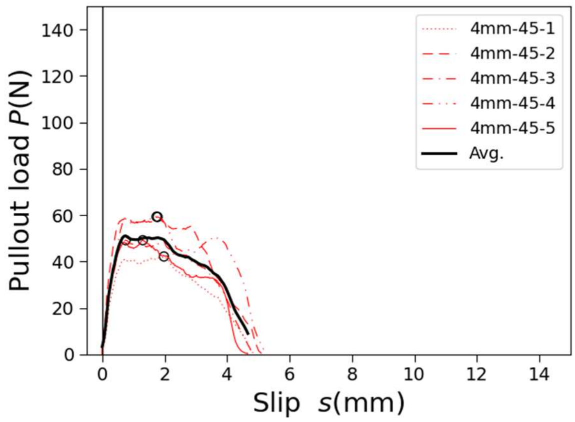

(d)

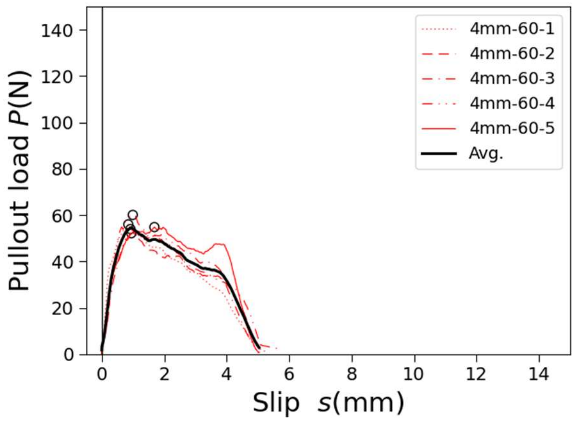

(e)

Fig. 3.7 Pullout load-slip relationship:
(Matrix strength of Fc36, Embedded length of 4mm)
(a)Inclined angle 0°, (b) Inclined angle 15°, (c) Inclined angle 30°,
(d) Inclined angle 45°, (e) Inclined angle 60°

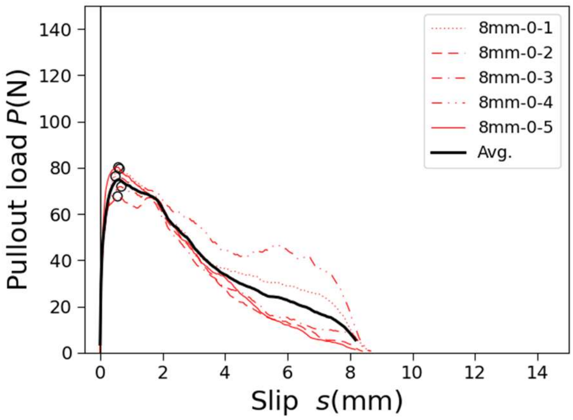

(a)

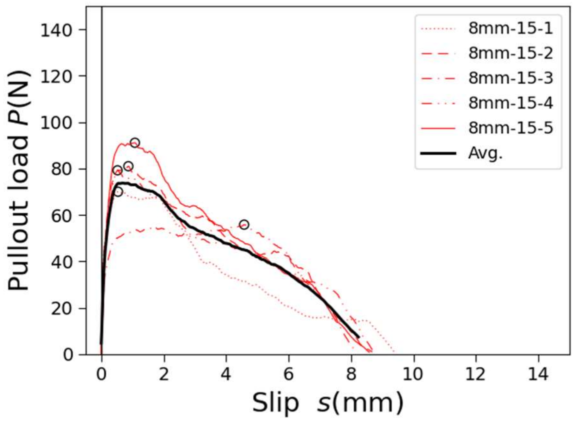

(b)

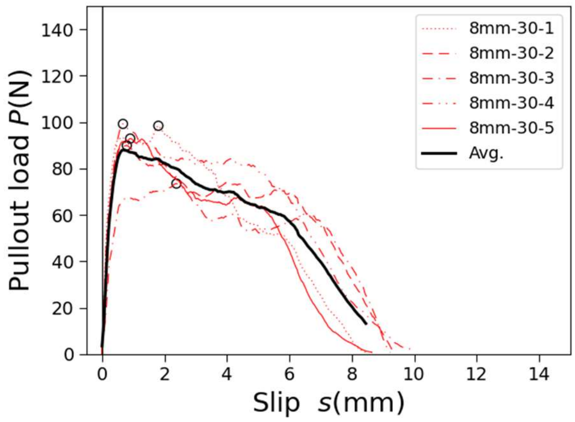

(c)

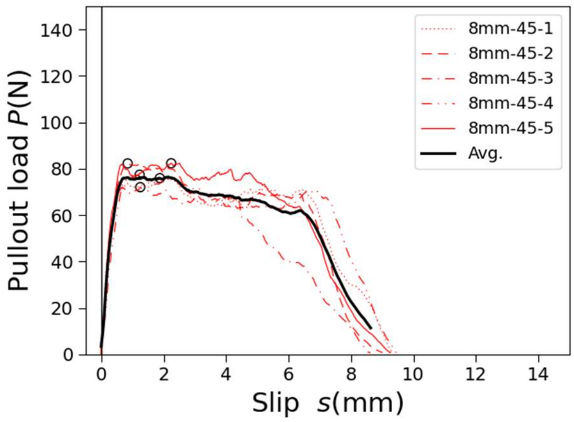

(d)

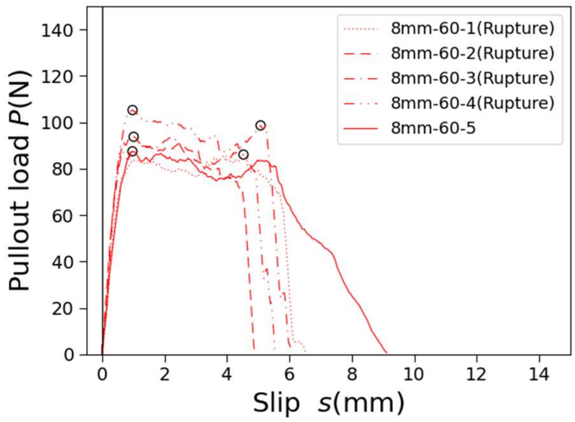

(e)

Fig. 3.8 Pullout load-slip relationship:
(Matrix strength of Fc36, Embedded length of 8mm)
(a)Inclined angle 0°, (b) Inclined angle 15°, (c) Inclined angle 30°,
(d) Inclined angle 45°, (e) Inclined angle 60°

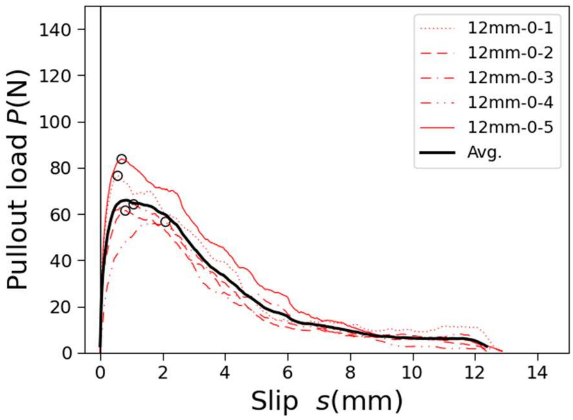

(a)

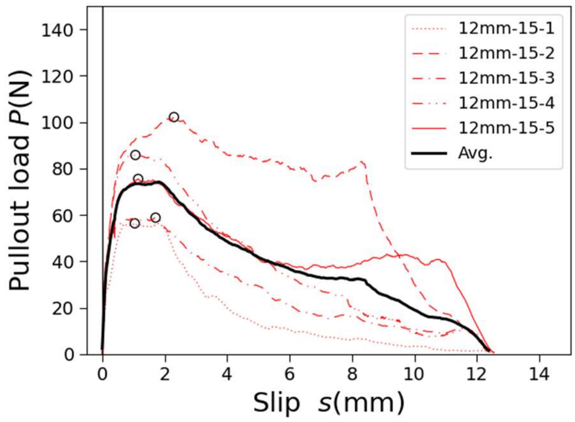

(b)

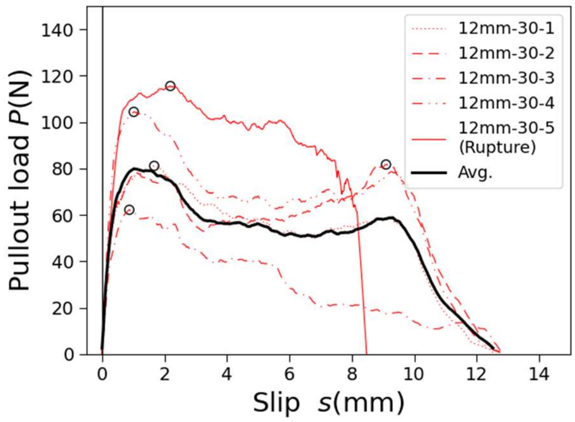

(c)

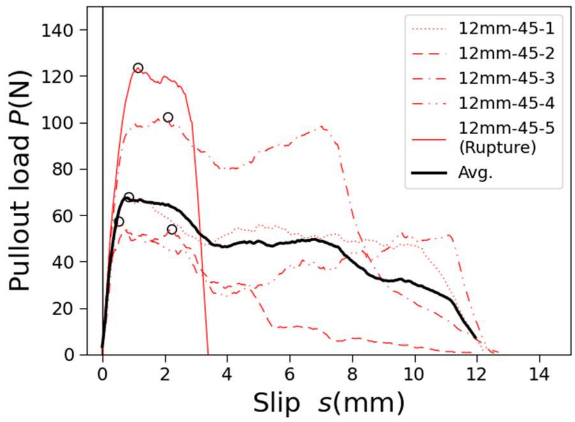

(d)

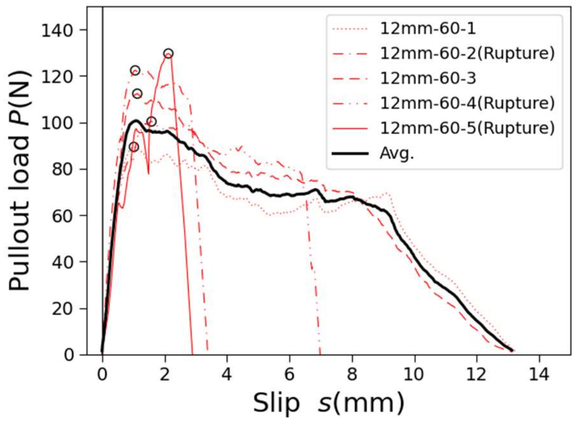

(e)

Fig. 3.9 Pullout load-slip relationship:
(Matrix strength of Fc36, Embedded length of 12mm)
(a)Inclined angle 0°, (b) Inclined angle 15°, (c) Inclined angle 30°,
(d) Inclined angle 45°, (e) Inclined angle 60°

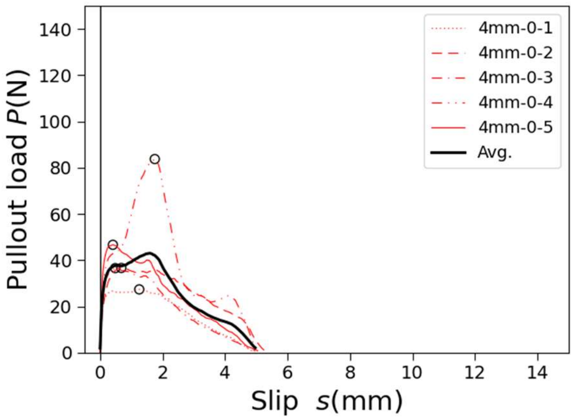

(a)

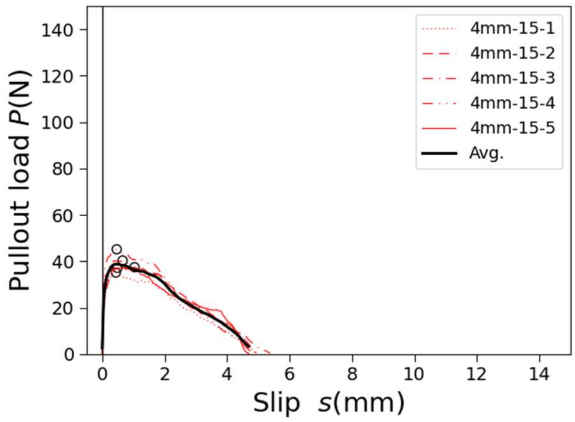

(b)

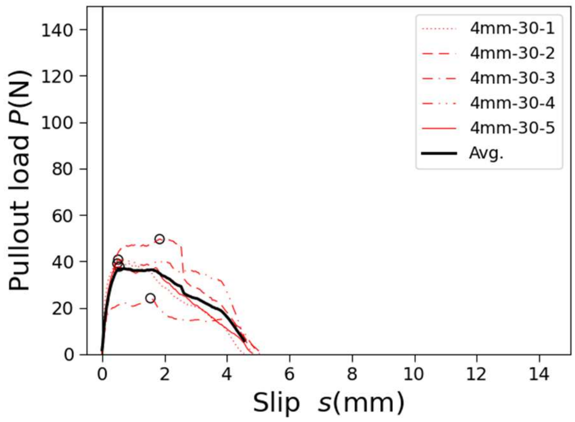

(c)

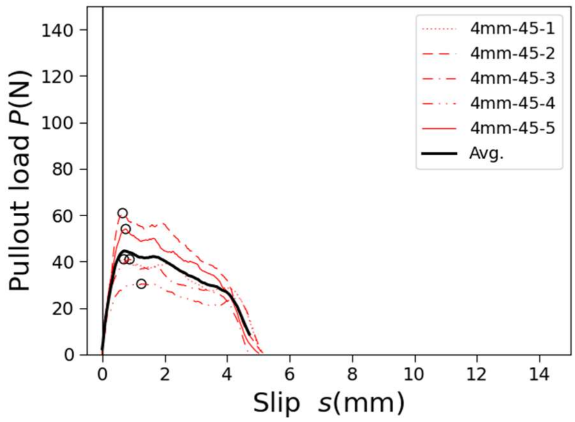

(d)

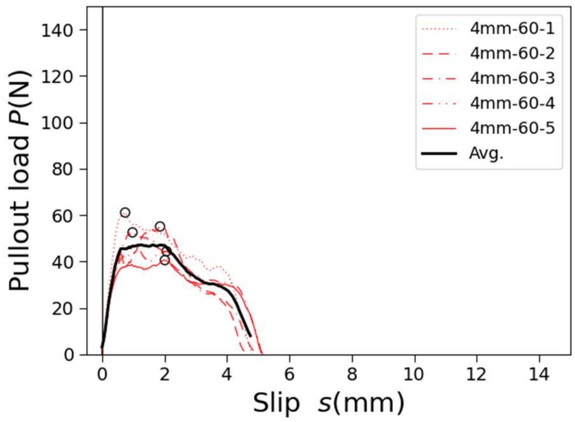

(e)

Fig. 3.10 Pullout load-slip relationship:
(Matrix strength of Fc48, Embedded length of 4mm)
(a)Inclined angle 0°, (b) Inclined angle 15°, (c) Inclined angle 30°,
(d) Inclined angle 45°, (e) Inclined angle 60°

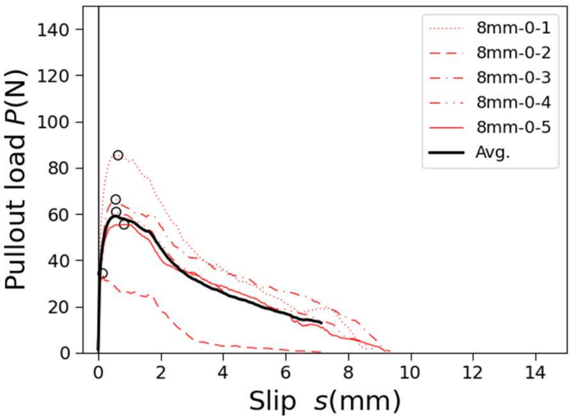

(a)

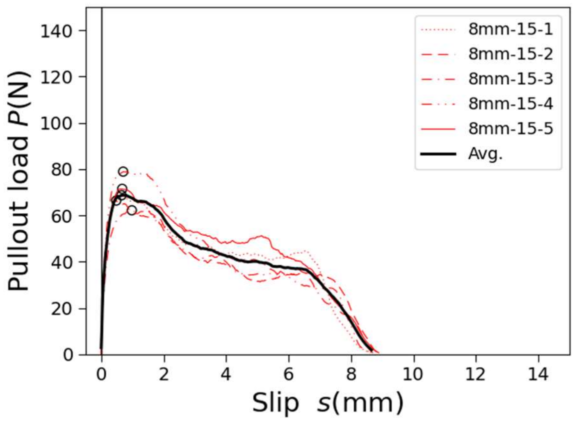

(b)

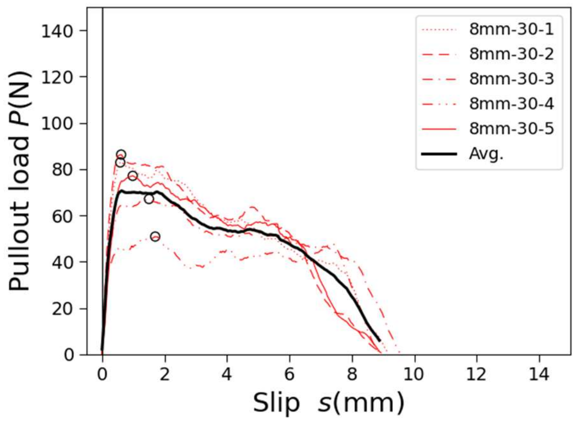

(c)

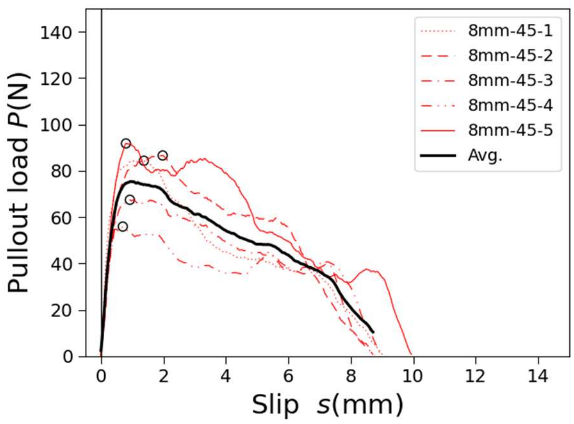

(d)

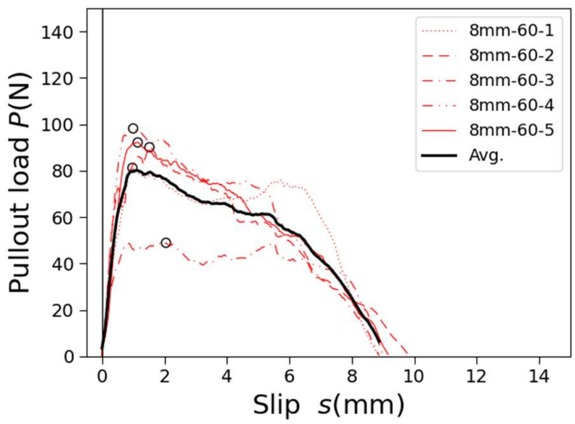

(e)

Fig. 3.11 Pullout load-slip relationship:
(Matrix strength of Fc48, Embedded length of 8mm)
(a)Inclined angle 0°, (b) Inclined angle 15°, (c) Inclined angle 30°,
(d) Inclined angle 45°, (e) Inclined angle 60°

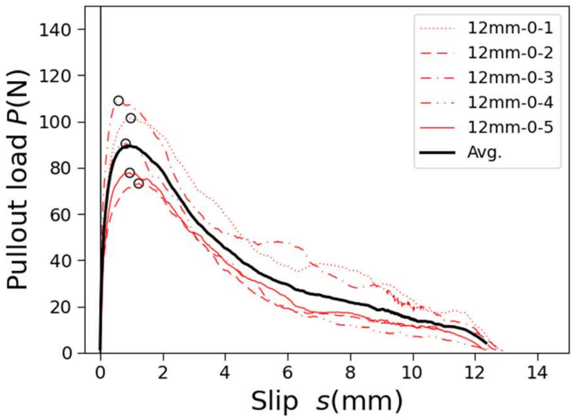

(a)

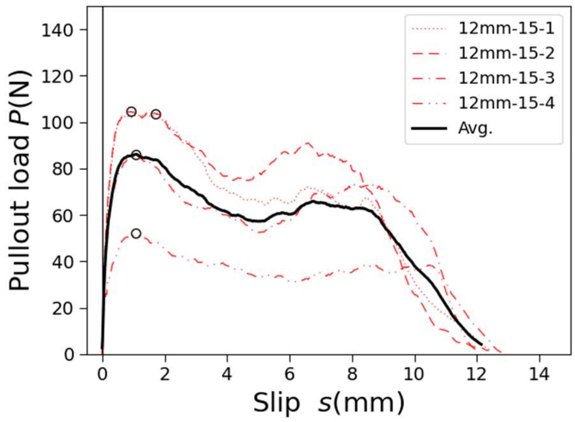

(b)

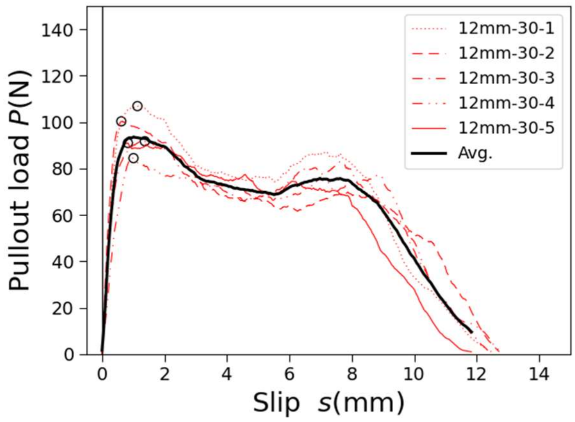

(c)

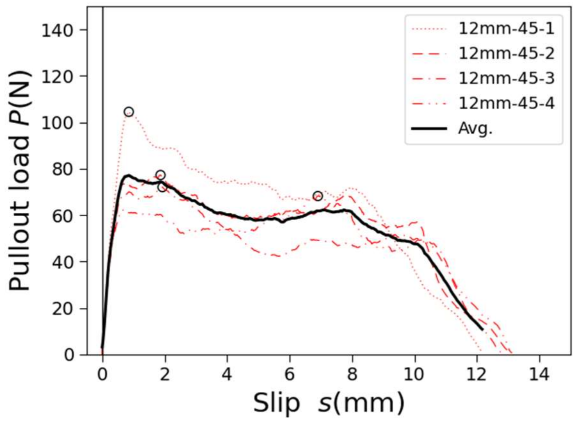

(d)

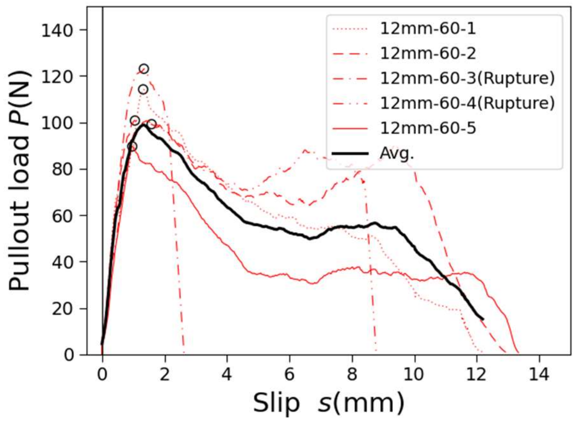

(e)

Fig. 3.12 Pullout load-slip relationship:
(Matrix strength of Fc48, Embedded length of 12mm)
(a)Inclined angle 0°, (b) Inclined angle 15°, (c) Inclined angle 30°,
(d) Inclined angle 45°, (e) Inclined angle 60°

Chapter 4 Discussions of Results

4.1 Bilinear Model of Pullout Load – Slip Curve

4.1.1 Method of modeling

From the relationship of pullout load-slip, two properties of the pullout behavior of bundled aramid fibers are found from the curves: a high stiffness at the preliminary stage, and a gently decreasing of pullout load after the maximum. Thus, the bilinear model is applied to evaluate the relationship between pullout load and slip to obtain an accurate result.

Details of the constitution of the bilinear model are shown in **Fig. 4.1** as same as previous study [12]. The bilinear model describes three characteristic points: the maximum load and slips at the maximum and the load becomes zero.

The maximum pullout load of the average curves for each test series is directly used for modeling. The complementary energy is considered for the calculation for the slip at the maximum load. As shown in **Fig. 4.1**, the slip is calculated as the maximum is reached at the line of which the complementary energy is equal. The pullout load is almost null when the slip is equal embedded length of the fiber. Therefore, the slip at this point was set to zero in the model. The example of the model is shown in **Fig. 4.2**.

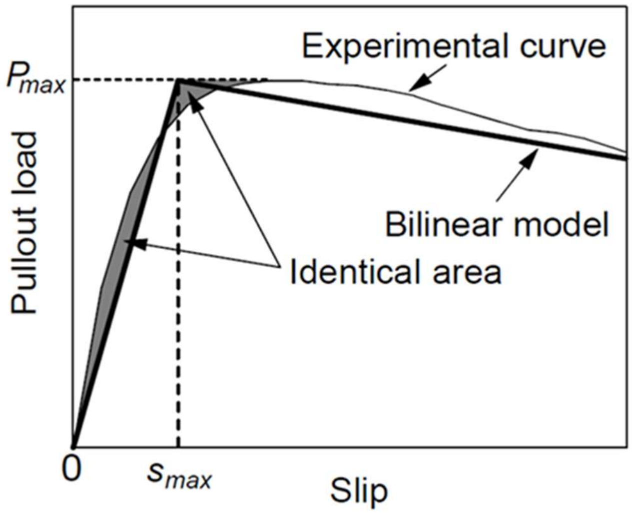

Fig. 4.1 Bilinear model [12]

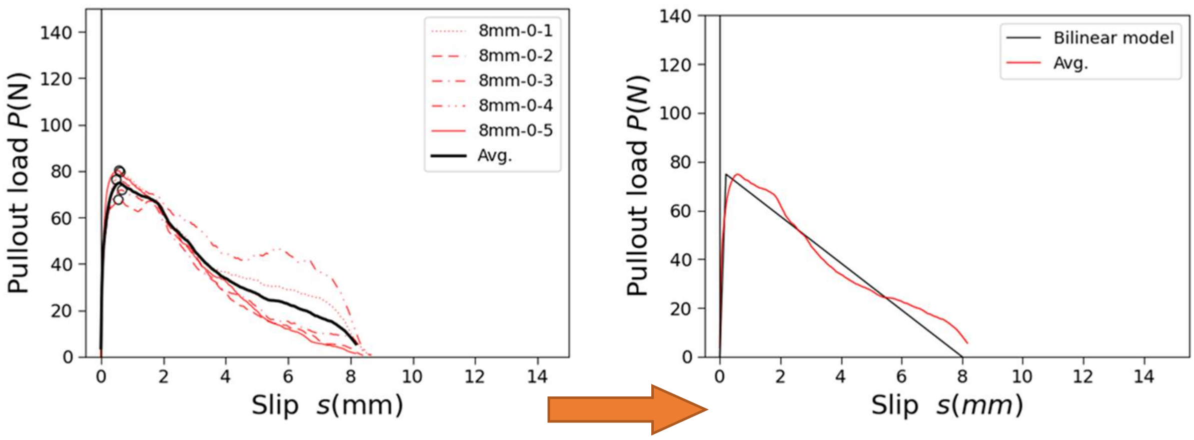

(a) **(b)**

Fig. 4.2 Example of bilinear model:
(a)Experiment result, (b)Model result

4.1.2 Modeling Results

Table 4.1 to **Table 4.3** summarizes the result of bilinear modeling. The embedded length in the table is calculated with average value of the thickness of the specimens. The maximum pullout load P_{max} and the slip at the maximum pullout load s_{max} are obtained from the average curves of each test series. $s_{c,max}$ express the calculated slip at the maximum load s_{max} using the bilinear model. "○" indicates specimen with ruptured fiber during loading.

Table 4.1 List of modeling results
(Matrix strength of Fc24)

Specimen Designation	Inclined Angle (°)	Embedded Length (mm)	s_{max} (mm)	P_{max} (N)	$s_{c,max}$ (mm)	Fiber Rupture
Fc24-4mm-0	0	3.97	1.45	20.85	0.22	
Fc24-4mm-15	15	3.97	0.37	24.90	0.14	
Fc24-4mm-30	30	3.91	0.62	25.30	0.29	
Fc24-4mm-45	45	3.91	1.04	34.42	0.47	
Fc24-4mm-60	60	3.97	1.26	35.76	0.79	
Fc24-8mm-0	0	7.95	0.81	30.77	0.34	
Fc24-8mm-15	15	8.01	0.75	41.47	0.27	
Fc24-8mm-30	30	7.96	0.62	31.99	0.35	
Fc24-8mm-45	45	7.98	1.10	41.87	0.61	
Fc24-8mm-60	60	7.97	1.22	40.57	0.72	
Fc24-12mm-0	0	11.83	0.39	31.36	0.12	
Fc24-12mm-15	15	11.83	0.80	47.92	0.39	
Fc24-12mm-30	30	11.84	0.81	44.72	0.55	
Fc24-12mm-45	45	11.85	1.49	44.47	0.84	
Fc24-12mm-60	60	11.88	2.27	56.59	1.62	

Table 4.2 List of modeling results
(Matrix strength of Fc36)

Specimen Designation	Inclined Angle (°)	Embedded Length (mm)	s_{max} (mm)	P_{max} (N)	$s_{c,max}$ (mm)	Fiber Rupture
Fc36-4mm-0	0	4.01	0.41	37.30	0.14	
Fc36-4mm-15	15	4.06	0.76	40.82	0.26	
Fc36-4mm-30	30	4.02	1.64	41.74	0.41	
Fc36-4mm-45	45	4.01	0.73	51.01	0.50	
Fc36-4mm-60	60	4.04	0.92	54.54	0.61	
Fc36-8mm-0	0	8.02	0.60	74.86	0.20	
Fc36-8mm-15	15	8.01	0.68	73.71	0.27	
Fc36-8mm-30	30	8.03	0.68	87.98	0.40	
Fc36-8mm-45	45	8.03	2.13	76.43	0.51	
Fc36-8mm-60	60	8.02	0.97	87.48	0.71	○
Fc36-12mm-0	0	11.84	0.84	65.96	0.30	
Fc36-12mm-15	15	11.91	1.81	74.24	0.47	
Fc36-12mm-30	30	11.86	1.03	79.92	0.50	○
Fc36-12mm-45	45	11.89	0.78	67.39	0.50	○
Fc36-12mm-60	60	11.93	1.08	100.68	0.74	○

Table 4.3 List of modeling results
(Matrix strength of Fc48)

Specimen Designation	Inclined Angle (°)	Embedded Length (mm)	s_{max} (mm)	P_{max} (N)	$s_{c,max}$ (mm)	Fiber Rupture
Fc48-4mm-0	0	3.98	1.57	43.05	0.43	
Fc48-4mm-15	15	3.98	0.45	38.87	0.14	
Fc48-4mm-30	30	4.06	0.70	36.96	0.33	
Fc48-4mm-45	45	4.02	0.70	44.61	0.44	
Fc48-4mm-60	60	4.02	1.23	47.22	0.53	
Fc48-8mm-0	0	8.04	0.56	59.21	0.18	
Fc48-8mm-15	15	8.03	0.72	68.80	0.27	
Fc48-8mm-30	30	8.09	0.63	70.65	0.38	
Fc48-8mm-45	45	8.05	0.94	75.36	0.50	
Fc48-8mm-60	60	8.04	1.10	80.15	0.67	
Fc48-12mm-0	0	11.90	0.94	89.46	0.30	
Fc48-12mm-15	15	11.90	1.09	86.14	0.36	
Fc48-12mm-30	30	11.86	1.02	93.57	0.52	
Fc48-12mm-45	45	11.87	0.85	77.14	0.52	
Fc48-12mm-60	60	11.87	1.33	98.93	0.87	○

4.2 Maximum Pullout Load

Fig. 4.3 shows the maximum pullout load comparison in three different matrix strengths at inclined angle 0°.

In general, the maximum pullout load increases as the strength of the matrix increases. Interestingly, the maximum pullout load is observed to increase significantly with the fiber's embedded length of 12mm. However, a slight increase of the maximum pullout load is observed when the fiber's embedded length is 4mm. In the case of fiber's embedded length of 8mm, the maximum pullout load even decreases as the matrix strength becomes stronger. This indicated that, for bundled aramid fibers, a stronger matrix strength can provide more benefits in enhancing the bond strength on fiber-cement interface. Furthermore, an adequate embedded length of the fiber can further exploit this advantage.

More details for the comparison at the other inclined angles are shown from **Fig 4.4(a)** to **Fig4.4(d)**.

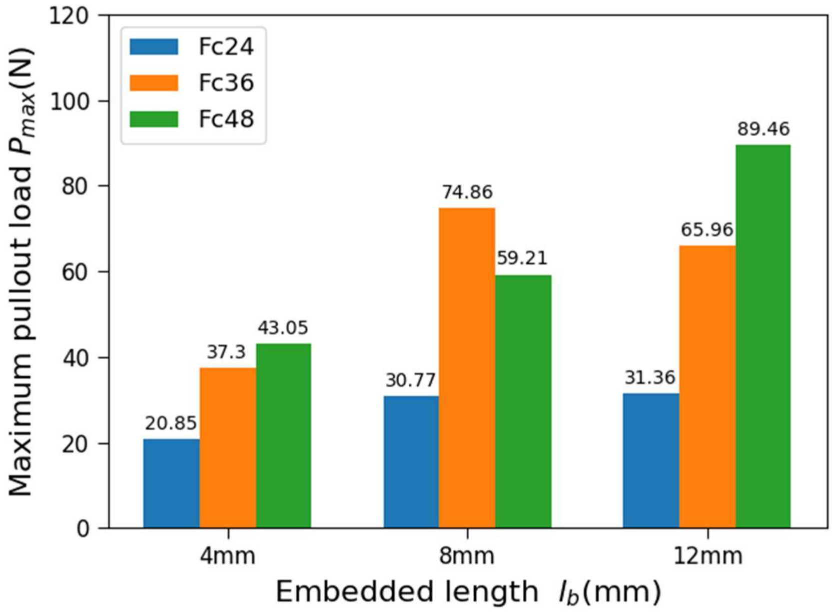

Fig. 4.3 Maximum pullout load in different matrix strengths (At inclined angle 0°)

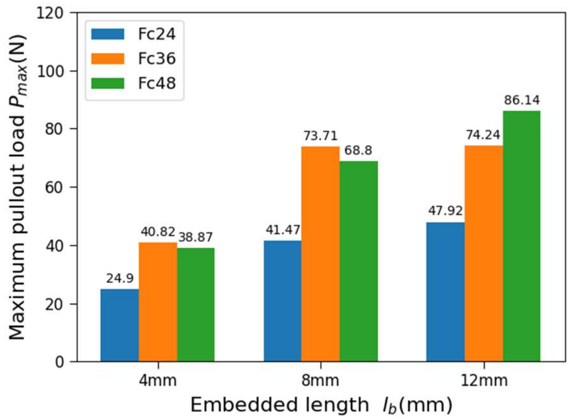

(a)

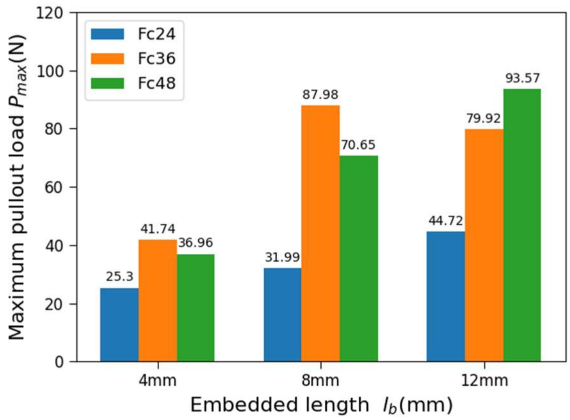

(b)

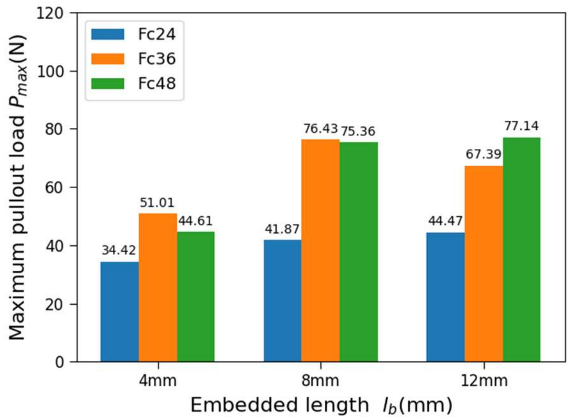

(c)

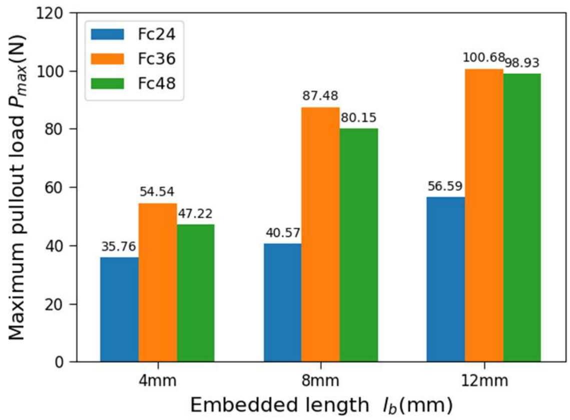

(d)

Fig. 4.4 Maximum pullout load in different matrix strengths:
(a)Inclined angle 15°, (b)Inclined angle 30°, (c)Inclined angle 45°, (d)Inclined angle 60°

4.3 Influence of Embedded Length

4.3.1 Pullout Load and Slip at Maximum Load

Based on the result from **Table 4.1** to **Table 4.3**, **Fig 4.5** compares the relationship between the maximum pullout P_{max} and the embedded length l_b of fibers with different matrix strength.

Fig 4.5 reveals that, the maximum pullout load generally increase as the embedded length becomes larger for all strength of the matrix. For the matrix strength of Fc48, a linear relationship is observed in most cases. However, in the matrix strength of Fc36, the relationship is quite unclear.

The same evaluation method is conducted for the slip at the maximum pullout load $s_{c,max}$, as shown in **Fig. 4.6**. The slip at the maximum pullout load $s_{c,max}$ is obtained by bilinear modeling.

As shown in **Fig 4.4**, data are slightly scattered in Fc24 and Fc48. Moreover, the ultimate slip $s_{c,max}$ increases when the embedded length l_b is longer, which showing a similar tendency than P_{max}.

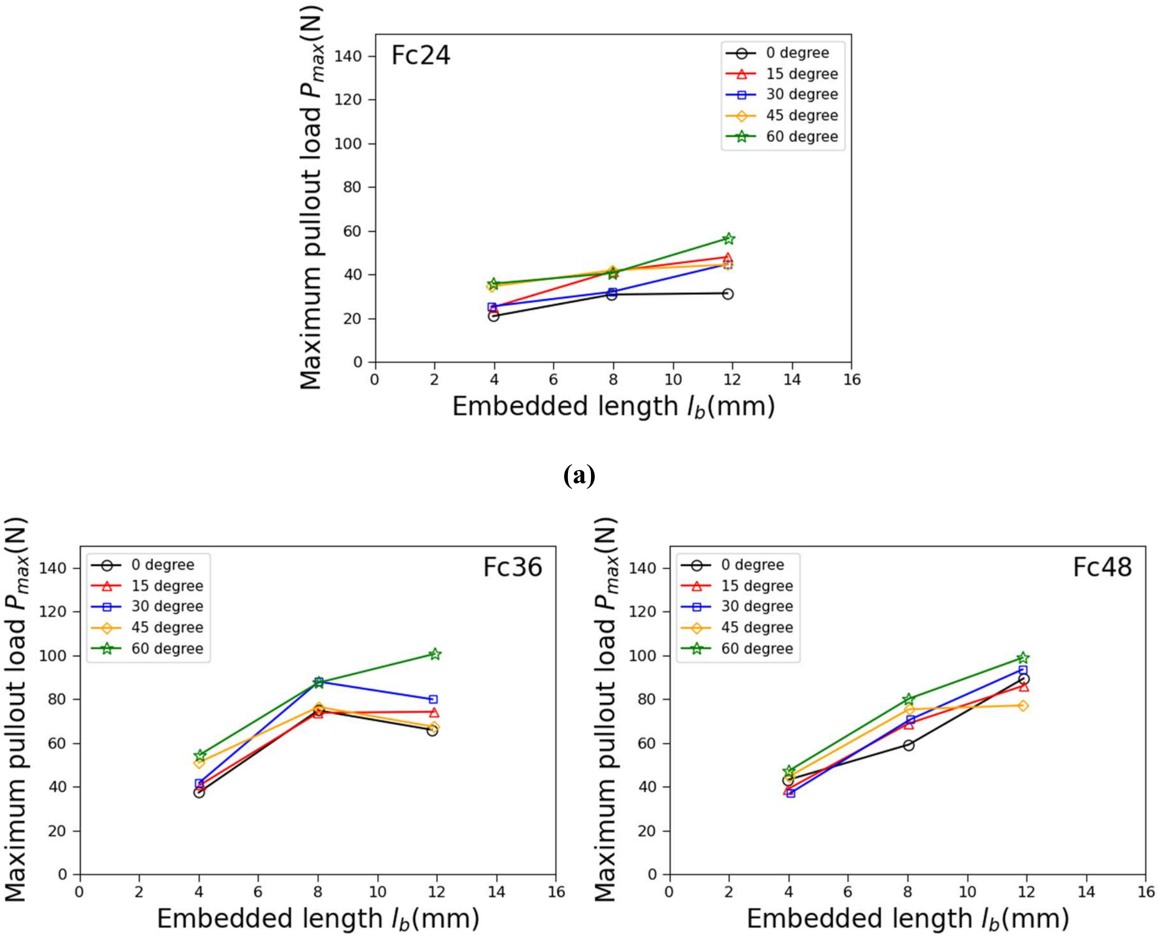

(a)

(b) **(c)**

Fig. 4.5 Relationship between maximum pullout load and embedded length: (a)Matrix strength of Fc24, (b)Matrix strength of Fc36, (c)Matrix strength of Fc48

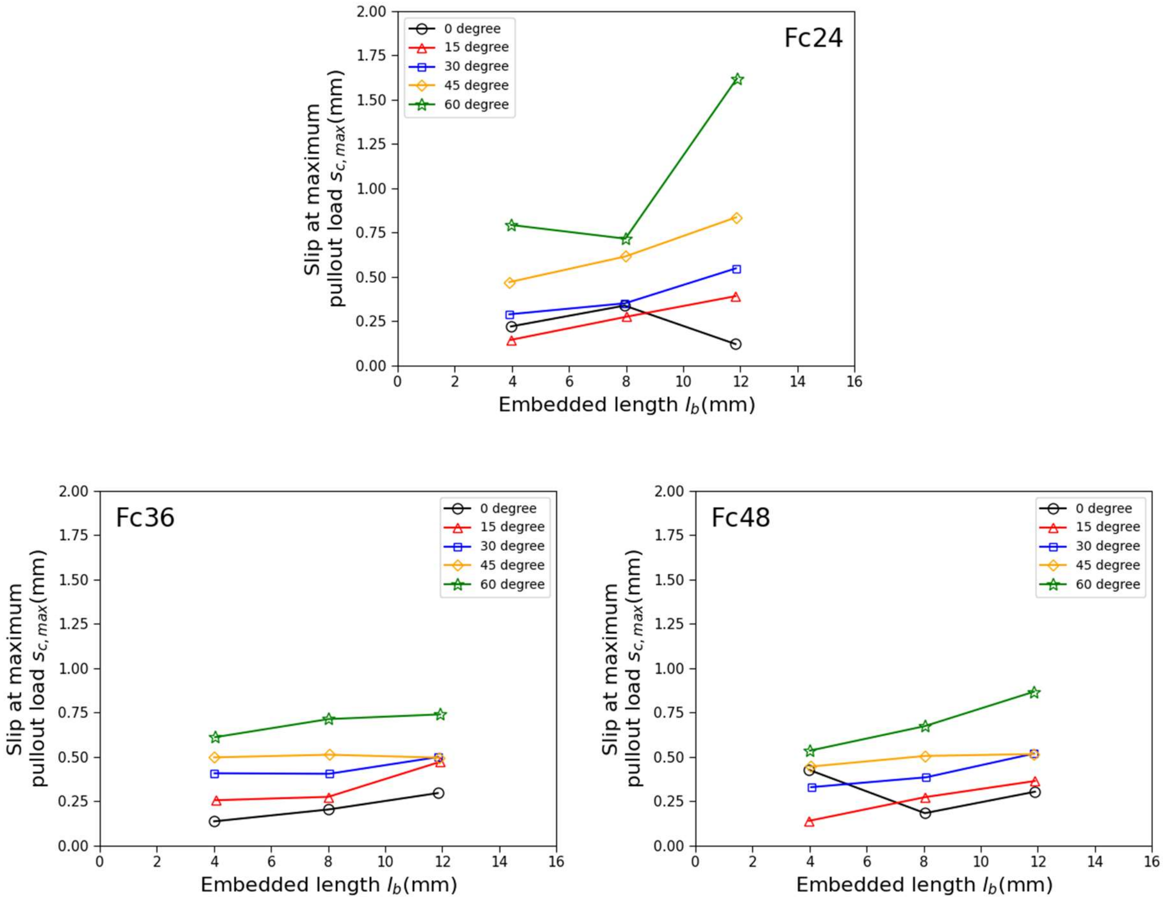

Fig. 4.6 Relationship between maximum pullout load and embedded length: (a)Matrix strength of Fc24, (b)Matrix strength of Fc36, (c)Matrix strength of Fc48

4.3.2 Evaluation formulas

(1)Evaluation of maximum pullout load

Several reports have investigated the relationship between the maximum pullout load and the embedded length of the fiber. Kanda and Li [6] conducted pullout test for the PVA fiber in a cementitious matrix. They suggested a linear relationship between the peak load and embedded length, as shown in **Fig 4.7**.

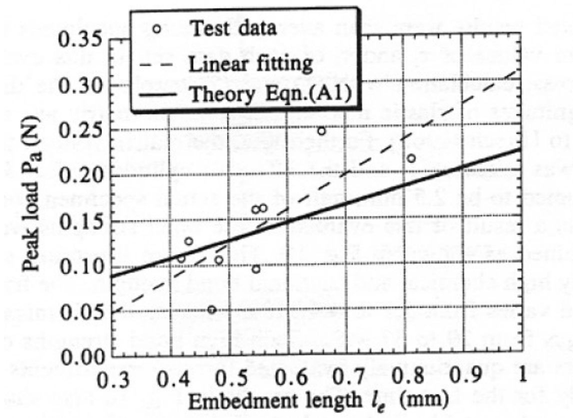

Fig. 4.7 Comparison of peak pullout from literature

Takaku and Arridge [13] conducted a pullout test for the stainless fibers in an epoxy resin matrix. They proposed a hyperbolic tangent function relationship between the debonding stress and embedded length as shown in **Fig. 4.8**. The debonding stress is defined as the peak load per unit cross-sectional area, the hollow plots and the solid plots represent test values for clean wire and coated wire, respectively. The coated wire is coated with a mold release agent to obtain a poor bonding and low friction property at the interface. In this study, a nearly power function relationship is found between debonding stress and embedded length.

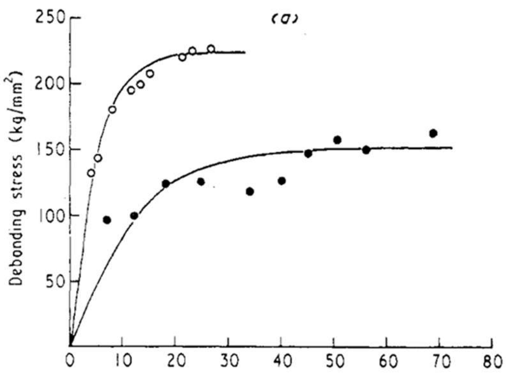

(x-axis: Embedded length (mm))

Fig. 4.8 Debonding stress versus embedded length

In this study, the relationship between the maximum pullout load P_{max} and embedded length l_b is evaluated by using specimens at the inclined angle of 0°. The least square method is adopted to fit the data with a power function, as shown in **Fig. 4.9**.

In general, the test results are in good agreements with the proposed model. With increasing of matrix strength, the empirical coefficient from the regression analysis increases. This indicates that the relationship of P_{max} and l_b have a linear tendency in high strength matrix. This is likely due to the fact that the good densification of the cementitious composite in high matrix strength can provide enough bonding stress on the interface matrix-fiber. On the other hand, the matrix Fc24 is damaged on the interface in case of long embedded length.

More details of this relationship for the specimens at an inclined angle are shown from **Fig.4.10** to **Fig. 4.12,** which show a similar tendency.

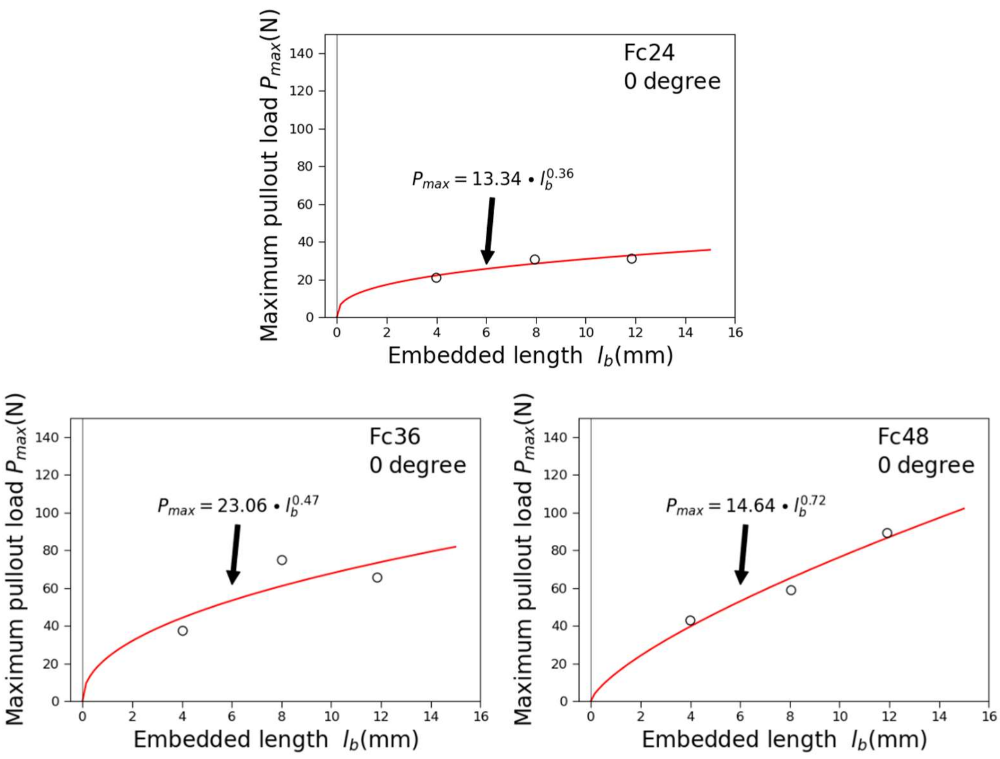

Fig. 4.9 Estimation of
maximum pullout load as function of embedded length at inclined angle 0°

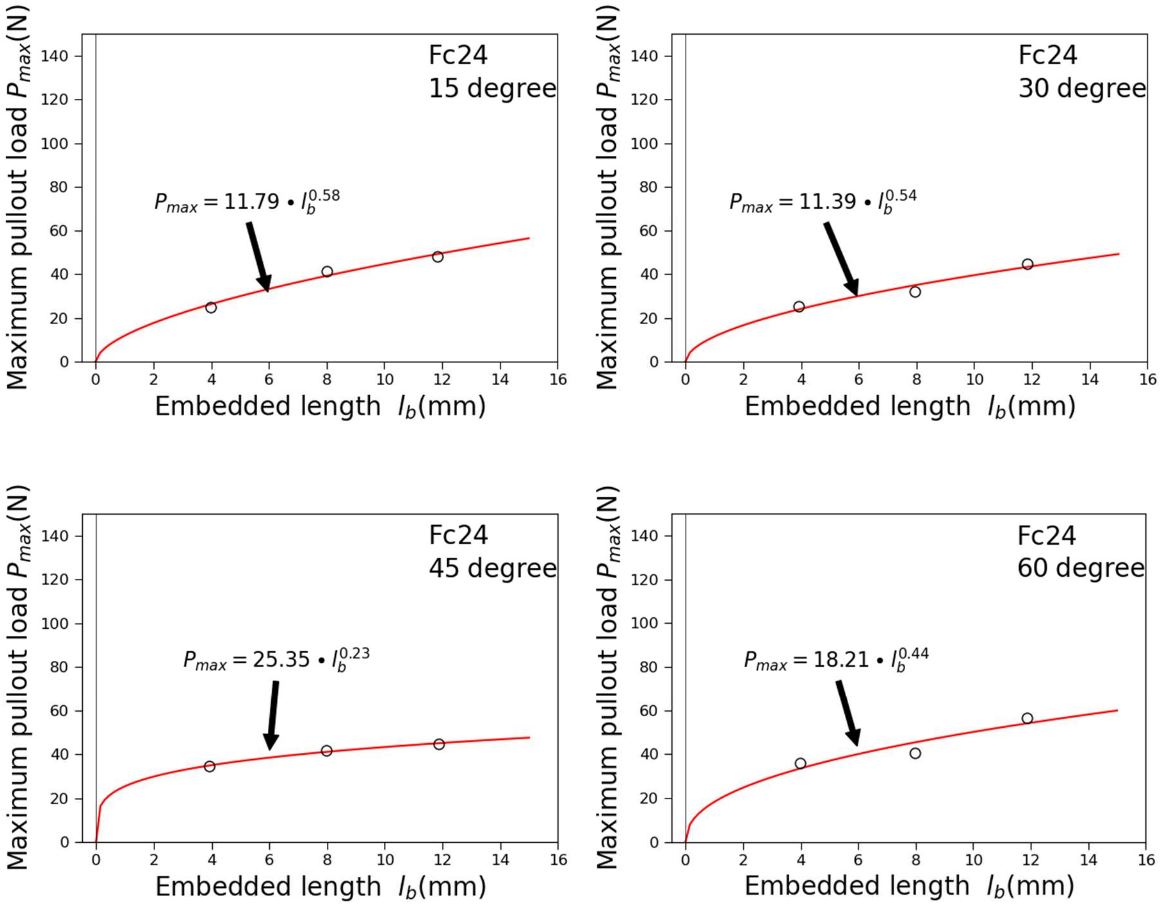

Fig. 4.10 Estimation of
maximum pullout load as function of embedded length at the inclined angle 15°-60°
(Matrix strength of Fc24)

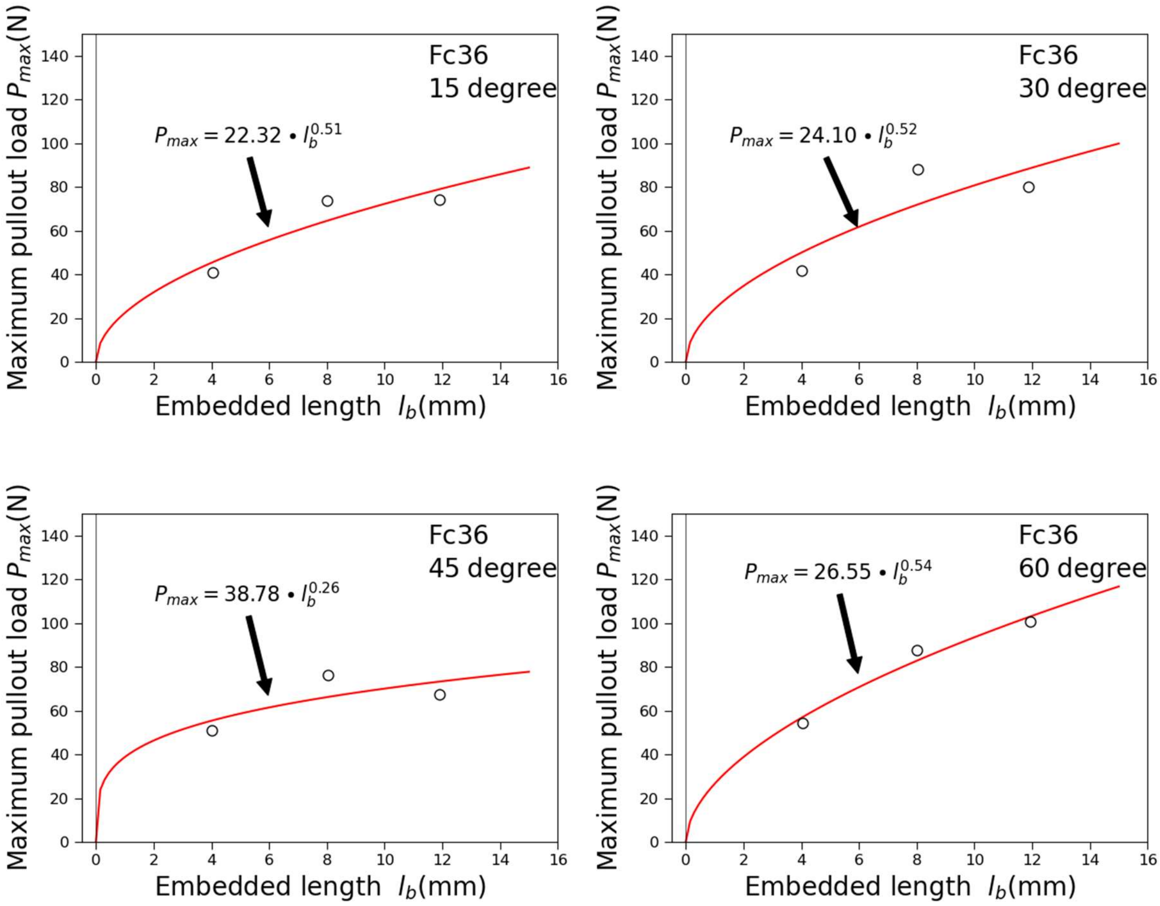

Fig. 4.11 Estimation of maximum pullout load as function of embedded length at the inclined angle 15°-60° (Matrix strength of Fc36)

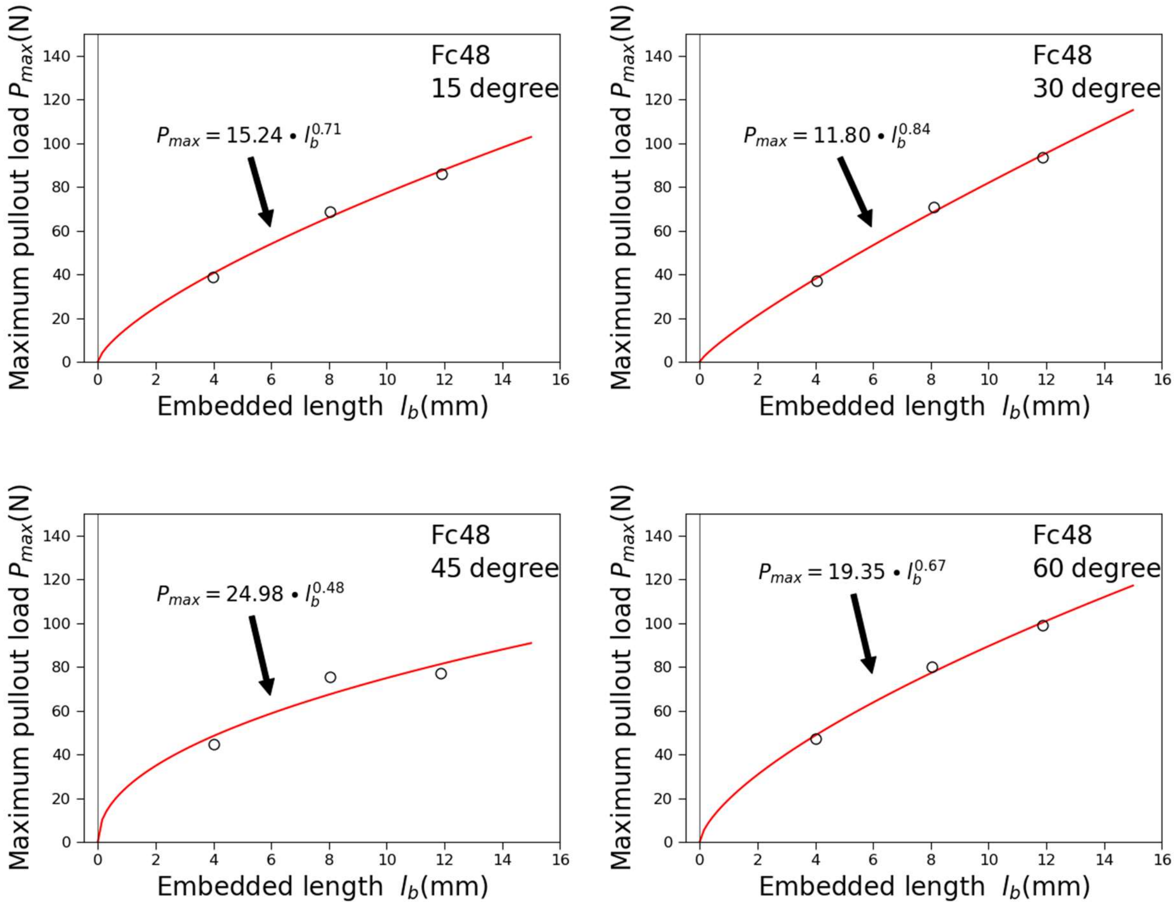

Fig. 4.12 Estimation of
maximum pullout load as function of embedded length at the inclined angle 15°-60°
(Matrix strength of Fc48)

(2) Estimation of the slip at the maximum pullout load

The similar method is conducted to evaluate the relationship between the slip at the maximum pullout load $s_{c,max}$ and the embedded length $l_b$by using specimens at the inclined angle of 0°. As shown in **Fig. 4.13**, linear approximate expressions are calculated by the least square method. Although the data scattering is observed, the test results show agreements with the predicted ones. The coefficient of the linear approximate expression increases with the increment of the matrix strength.

More details of this relationship for the specimens with an inclined angle are shown from **Fig.4.14** to **Fig. 4.16** which show a similar tendency.

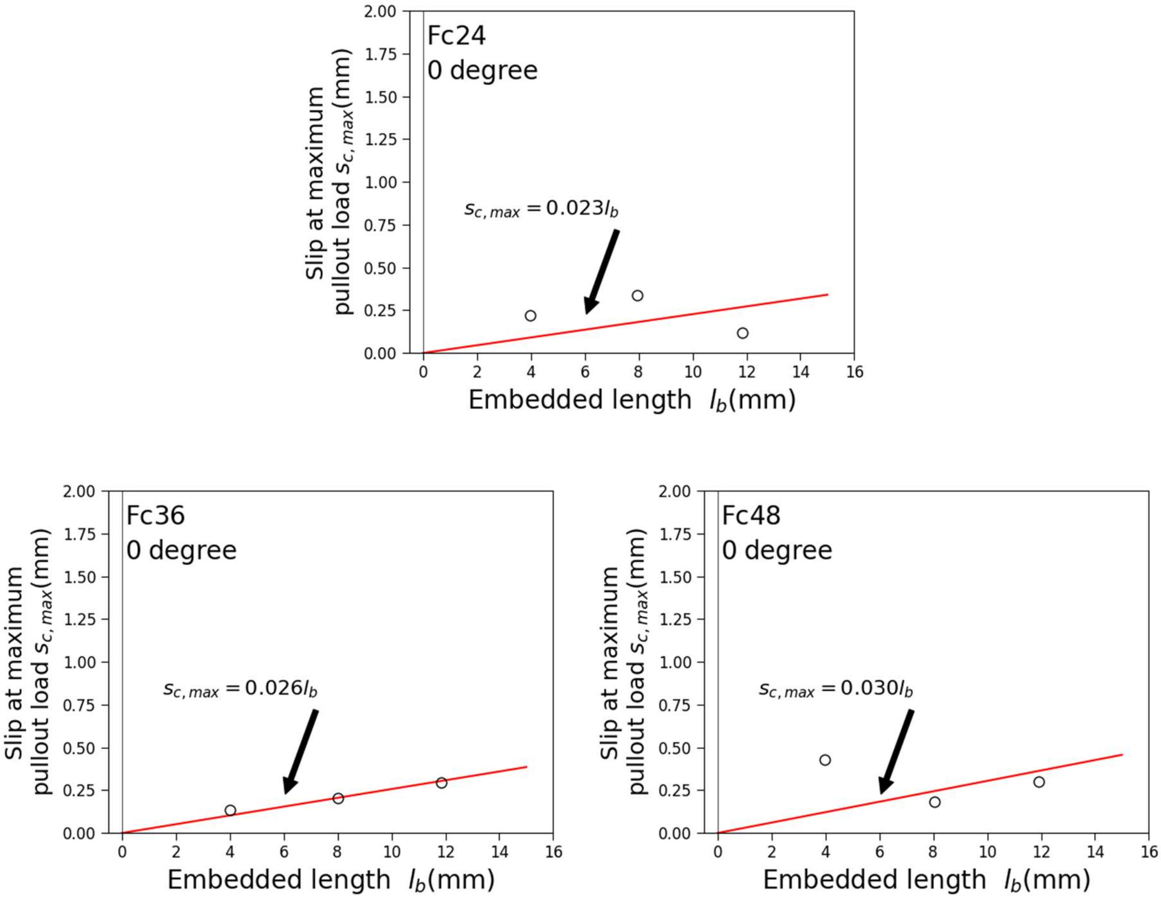

Fig. 4.13 Estimation of slip at the maximum pullout load as function of the embedded length at inclined angle 0°

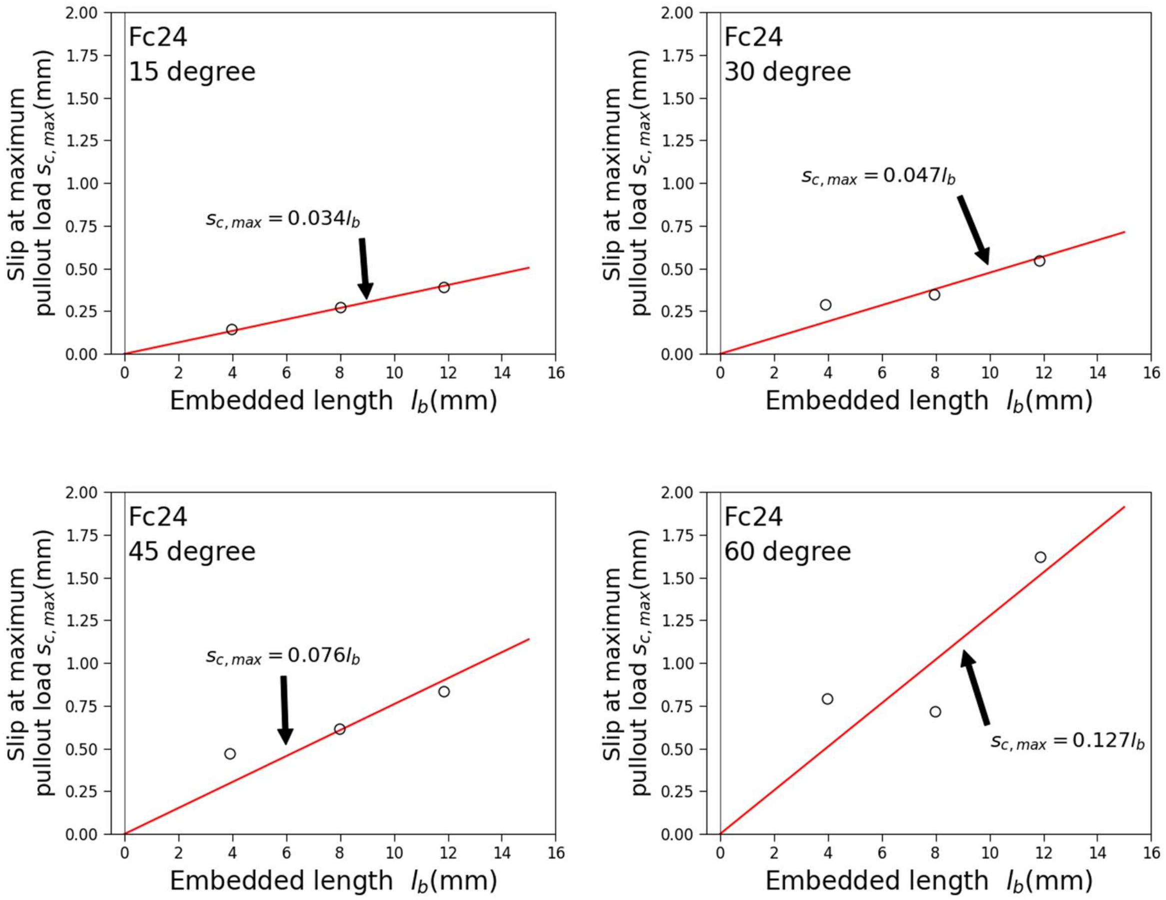

Fig. 4.14 Estimation of slip at the maximum pullout load as function of embedded length at the inclined angle 15°-60° (Matrix strength of Fc24)

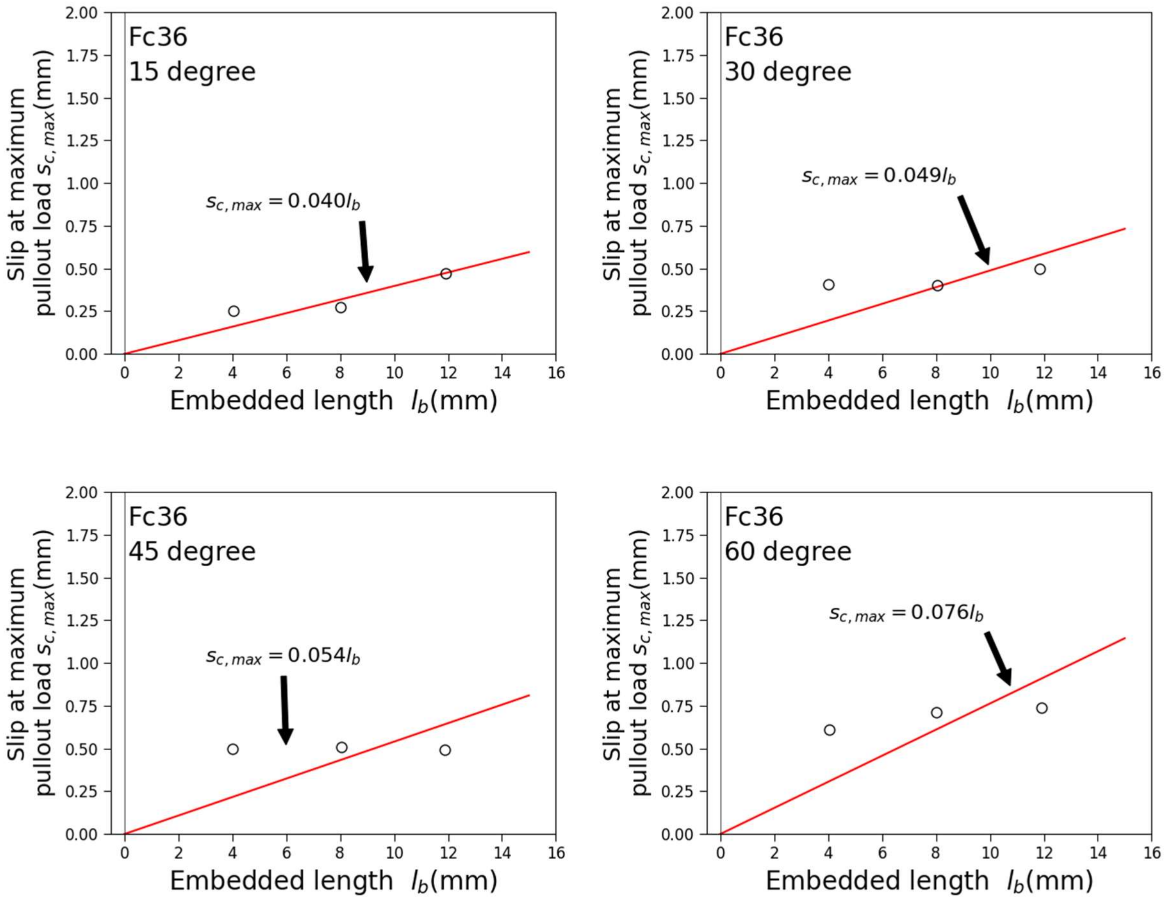

Fig. 4.15 Estimation of slip at the maximum pullout load as function of embedded length at the inclined angle 15°-60° (Matrix strength of Fc36)

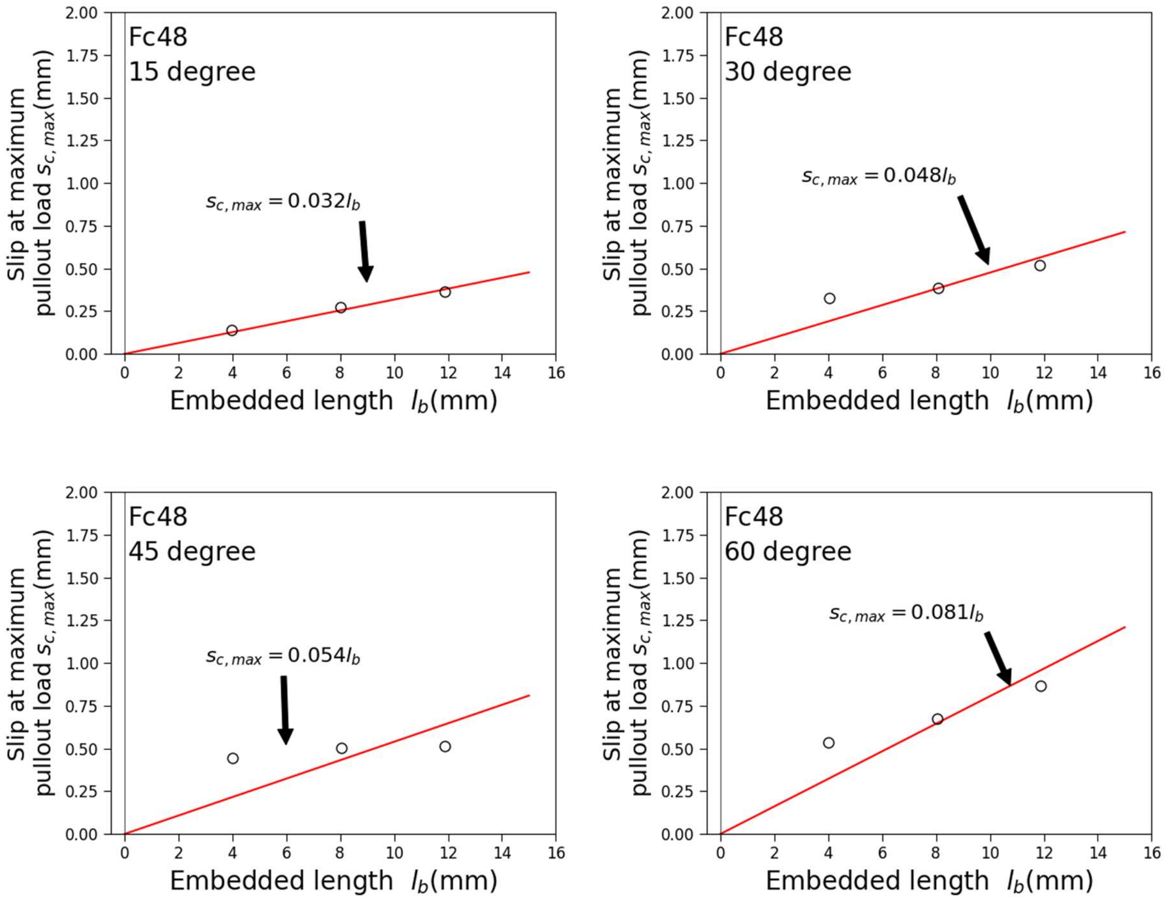

Fig. 4.16 Estimation of slip at the maximum pullout load as function of embedded length at the inclined angle 15°-60° (Matrix strength of Fc48)

4.4 Snubbing Effect

As Li et al. [5] demonstrated that the force of fiber pullout increase with the inclined angle of fiber. In this study, the snubbing effect is evaluated using the following Eq.(4.1)

$$P_{max} = P_{max,0} \cdot e^{f_p \cdot \theta} \tag{4.1}$$

Where,

P_{max}: maximum pullout load

$P_{max,0}$: P_{max} at inclined angle 0

f_p: coefficient of the snubbing effect for pullout load

θ: inclined angle

Fig. 4.17 shows the relationship of the normalized pullout load P_0 and the inclined angle θ. P_0 is the ratio of P_{max} to $P_{max,0}$. The fitting curve in the graph is obtained by the least square method. The unit of the inclined angle θ is in radian when calculating the coefficient related to the snubbing effect f_p.

From **Fig 4.17**, the coefficient of the snubbing effect f_p decreases as the matrix strength increases, indicates that the snubbing effect is difficult to exhibit in high matrix strength.

A similar method is conducted to evaluate the slip at the maximum pullout load following Eq.(4.2).

$$s_{c,max} = s_{c,max,0} \cdot e^{f_s \cdot \theta} \tag{4.2}$$

Where,

$s_{c,max}$: slip at the maximum pullout load

$s_{c,max,0}$: $s_{c,max,0}$ at inclined angle 0

f_s: coefficient of snubbing effect for slip at the maximum pullout load

θ: inclined angle

Fig. 4.18 shows the relationship between the normalized slip s_0 and the inclined angle θ. s_0 is the ratio of $s_{c,max}$ by $s_{c,max,0}$. A similar tendency of the coefficient f_s is observed that f_s decreases as the matrix strength becomes larger.

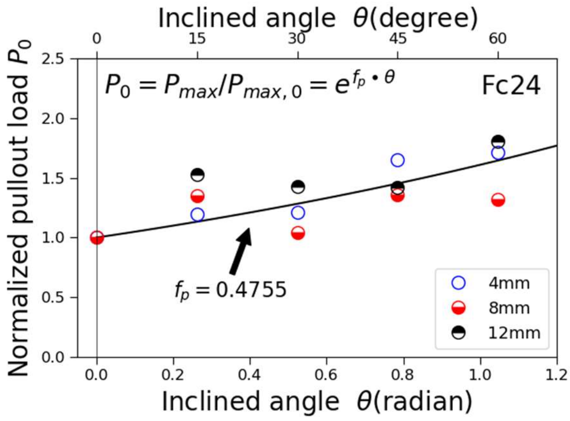

(a)

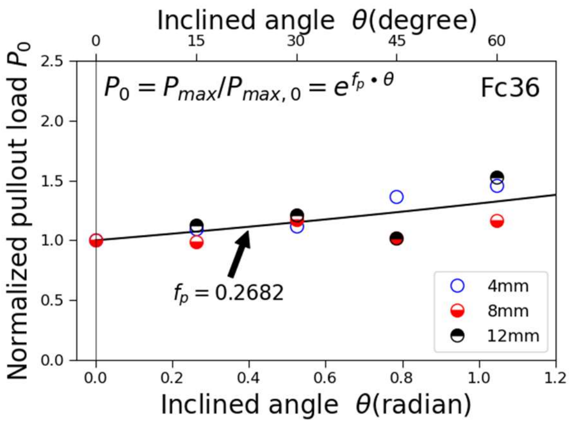

(b)

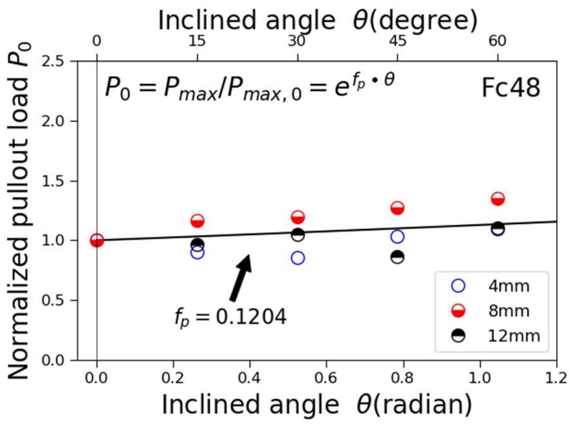

(c)

Fig. 4.17 Snubbing effect in normalized pullout load:
(a)Fc24 matrix strength, (b) Fc36 matrix strength, (c) Fc48 matrix strength.

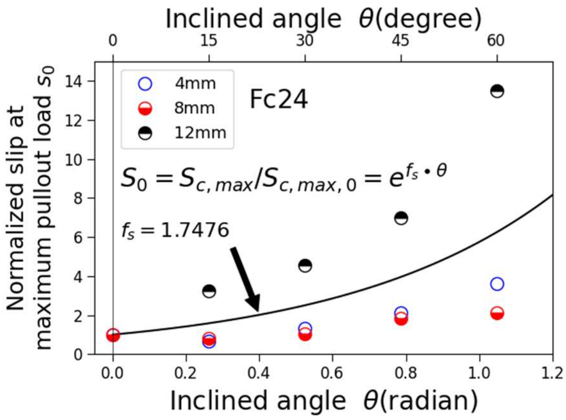

(a)

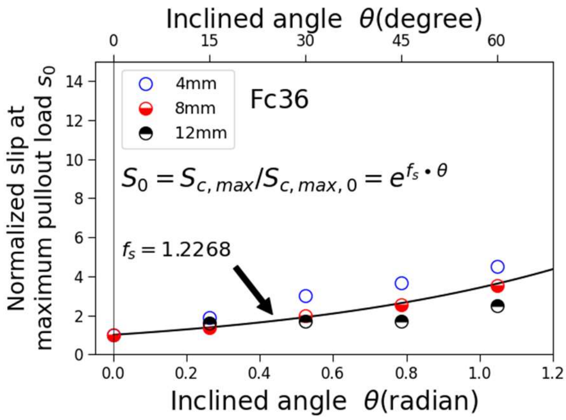

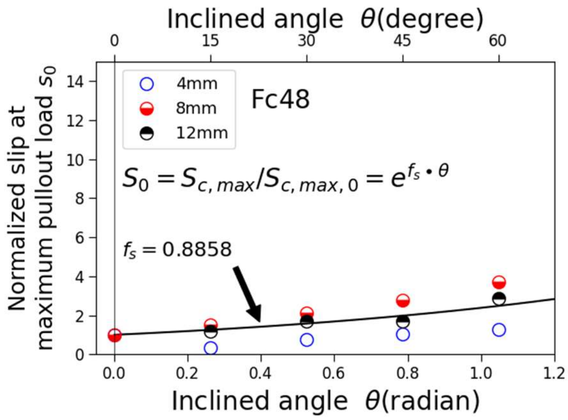

(b) **(c)**

Fig. 4.18 Snubbing effect in normalized slip at the maximum pullout load: (a)Fc24 matrix strength, (b) Fc36 matrix strength, (c) Fc48 matrix strength.

4.5 Apparent Strength of the Fiber

According to Kanda and Li [6], the reduction of the apparent strength of the fiber can be expressed as Eq(4.3),

$$\sigma_{fu} = \sigma_{fu}^{n} \cdot e^{-f' \cdot \phi} \tag{4.3}$$

Where:

σ_{fu}: apparent strength of fiber

σ_{fu}^{n}: rupture strength of the fiber at angle $\phi = 0$

f': apparent fiber strength reduction factor

ϕ: inclined angle

The relationship between the apparent fiber strength σ_{fu} and inclined angle ϕ is shown in **Fig. 4.19**. The coefficient f' represents the apparent fiber strength reduction factor which is obtained by the least square method. The nominal fiber strength σ_{fu}^{n} is defined as the rupture strength of the fiber when $\phi = 0$ in a cementitious matrix. The unit of the inclined angle θ is in radian when calculating the coefficient of the apparent strength of the fiber f'. As shown in **Fig.4.19**, the calculated values are almost constant indicating that the reduction of the apparent strength of the fiber cannot be evaluated in this study.

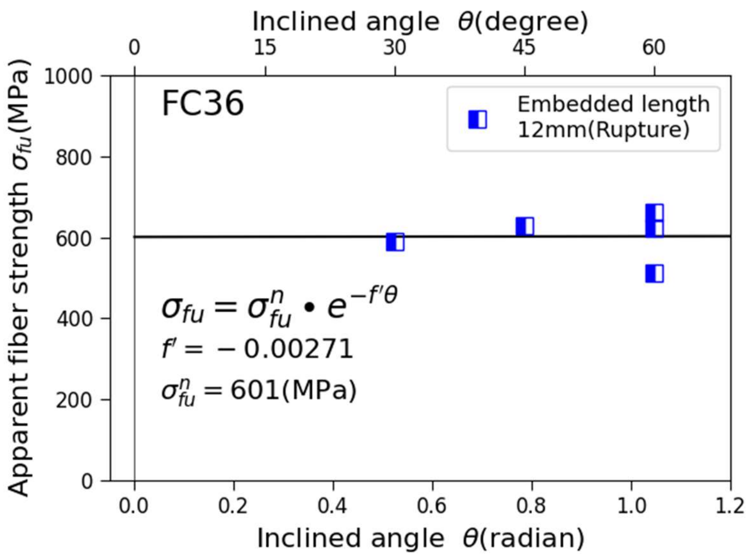

Fig. 4.19 Relationship between apparent strength and inclined angle

Chapter 5 Calculation of Bridging Law

5.1 Bilinear Model of Single-Fiber Pullout Behavior

Based on the discussions in the previous chapter, the single-fiber pullout model is summarized. At the inclined angle 0°, the maximum pullout load $P_{max,0}$ and the slip at the maximum pullout load $\delta_{c,max,0}$ are expressed by Eq.(5.1) and Eq.(5.2)

$$P_{max,0} = A \cdot l_b^B \tag{5.1}$$

$$\delta_{max,0} = C \cdot l_b \tag{5.2}$$

Where,

l_b: embedded length of the fiber

A, B, C: constant

The inclined angle strongly correlates the maximum pullout P_{max} and the slip at the maximum pullout load $s_{c,max}$, and can be calculated using Eq.(5.3) and Eq.(5.4).

$$P_{max} = P_{max,0} \cdot e^{f_p \cdot \theta} \tag{5.3}$$

$$\delta_{max} = \delta_{max,0} \cdot e^{f_s \cdot \theta} \tag{5.4}$$

Where,

θ: inclined angle

f_p: coefficient of the snubbing effect for pullout load

f_s: coefficient of the snubbing effect for slip

Thus, based on the P_{max} and δ_{max} obtained from the Eq.(5.1) to Eq.(5.4), and considering the behavior of the rupture of fibers, the bridging model of the single fiber can be expressed as the Eq.(5.5).

$$P(\delta, \theta, l_b) = \begin{cases} \frac{P_{max}}{\delta_{max}} \cdot \delta & (\delta \leq \delta_{max}) \\ P_{max} - \frac{P_{max}}{l_{b-\delta_{max}}} \cdot (\delta - \delta_{max}) & (\delta_{max} < \delta) \end{cases} \tag{5.5}$$

But,

$P(\delta, \theta, l_b) < A_f \cdot \sigma_{fu}$ (once exceed, $P = 0$)

Where,

A_f: cross-sectional area of fiber

σ_{fu}: apparent strength of fiber

5.2 Empirical Formulas

Based on the test results, several empirical formulas focusing on coefficient $A, B, C, f_p,\ and\ f_s$ are proposed, as shown in **Fig. 5.1**. The matrix strength based on the average value of uniaxial compression test results is used in the fitting. For coefficient A, a constant value on average is considered because it is difficult to predict the variation. For the other coefficients, a linear fitting calculated by the least square method is adopted. Overall, the calculated results are conservative. Thus, Eq.(5.6) to Eq.(5.9) are proposed based on the empirical formula.

$$P_{max,0} = 17.02 \cdot l_b^{0.0129\sigma_s + 0.0258} \tag{5.6}$$

$$\delta_{max,0} = (0.0002\sigma_s + 0.0170) \cdot l_b \tag{5.7}$$

$$P_{max} = P_{max,0} \cdot e^{(-0.0122\ \ {}_s + 0.7514)\cdot\,\theta} \tag{5.8}$$

$$\delta_{max} = \delta_{max,0} \cdot e^{(-0.029\ \ \ {}_s + 2.4075)\cdot\,\theta} \tag{5.9}$$

Where,

l_b: embedded length of the fiber

σ_s: matrix strength

θ: inclined angle

It should be noted that Eq.(5.6) to Eq.(5.9) are validated based on the hypothesis that these coefficients are influenced independently by σ_s. The application range is limited to the behavior of bundled aramid fibers in a cementitious matrix because completely different properties might be observed on different types of fiber or matrix. Also, because of the limitations of the experiment data, a non-linear relationship might be found in the matrix with much higher strength than in this experiment.

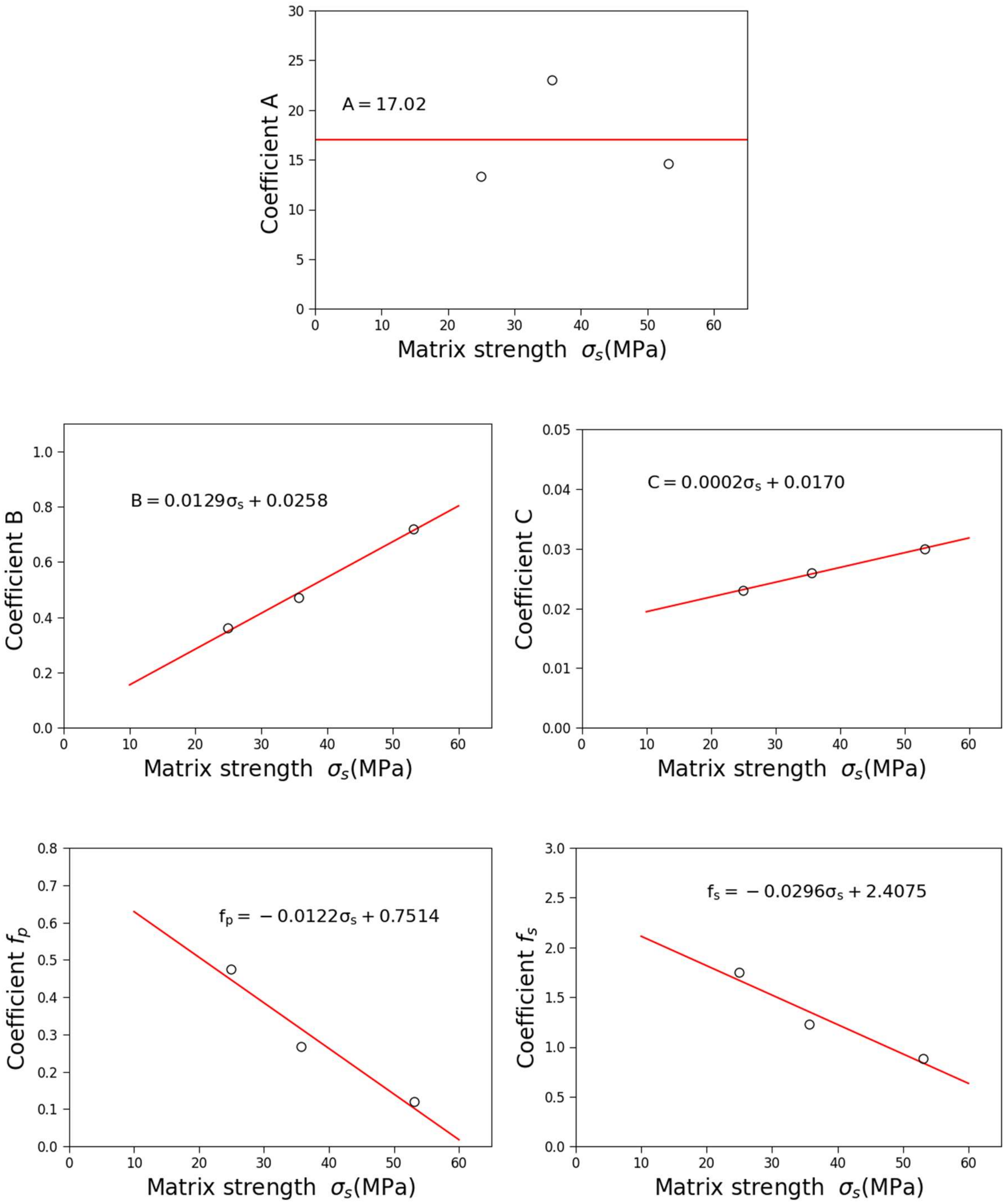

Figure 5.1 Linear fitting formula of the test result

5.3 Constitution of Bridging Law

The constitution of the bridging law is based on previous studies [2]. The bridging stress is defined as the total fiber pullout load divided by the cross-sectional area of the matrix. The fiber orientation distribution is expressed by adopting the elliptic distribution. The snubbing effect and the degradation of the apparent fiber strength are also considered in the calculation.

Fig. 5.2 shows the definitions of coordinate system and the fiber angle. The fiber angles, θ and ϕ, are the angles between the x-axis and the projected lines of the fiber(angle of Ψ to x-axis) to x-y and z-x planes. With the increment of the angle Ψ, the pullout load increases due to the snubbing effect. The elliptic distribution is considered for each of the x-y and z-x planes. Thus, the bridging stress can be expressed by Eq.(5.10).

$$\sigma_{bridge}(\delta) = \frac{P_{bridge}(\delta)}{A_m}$$

$$= \frac{V_f}{A_f} \cdot \sum_h \sum_j \sum_i P_{ij}(\delta, \Psi) \cdot p_{xy}(\theta_i) \cdot p_{zx}(\phi_j) \cdot p_x(y_h, z_h) \cdot \Delta\theta \cdot \Delta\phi \cdot (\Delta y \cdot \Delta z) \tag{5.10}$$

Where,

σ_{bridge}: bridging stress

P_{bridge}: bridging force(= total of pullout load)

A_m: cross-sectional area of the matrix

V_f: fiber volume friction

A_f: cross-sectional area of a fiber

$P_{ij}(\delta, \Psi)$: pullout load of single fiber

p_{xy}, p_{zx}: probability based on elliptic distribution

p_x: probability of fiber distribution along x-axis

Ψ: fiber angle to x-axis

θ: angle between x-axis and projected line of the fiber to x-y plane

ϕ: angle between x-axis and projected line of the fiber to z-x plane

The probability distribution function for elliptic distribution is expressed by Eq.(5.11)

$$p(\theta) = \frac{\sqrt{k}}{\pi} \cdot \frac{C}{\cos^2\theta + Asin\theta + Bsin^2\theta} \tag{5.11}$$

$$A = \frac{(1-k)sin2\theta_r}{1+(k-1)\sin^2\theta_r}$$

$$B = \frac{k-(k-1)\sin^2\theta_r}{1+(k-1)\sin^2\theta_r}$$

$$C = \frac{1}{1+(k-1)\sin^2\theta_r}$$

Where,

k: orientation intensity k

θ_r: principal orientation angle

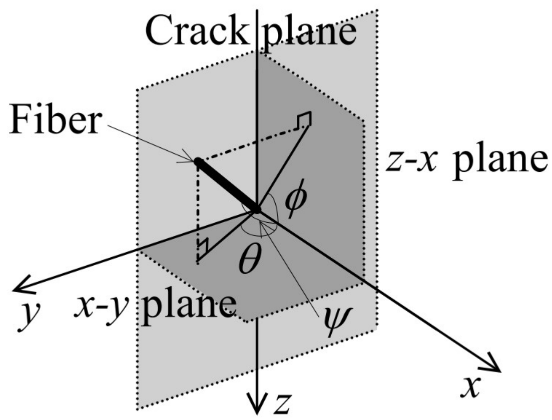

Fig. 5.2 Definitions of the coordinate system and fiber angle [12]

The input values for the calculation of the bridging law are shown in **Table 5.1**. The input values are calculated by fitting formulas shown in **Fig. 5.1**. The fiber volume fraction is set to 1%. The principal orientation angles are set to zero for calculation simplification. The width of the crack at the maximum load is set to be 1.5 times the slip at the maximum pullout load [12], and the orientation intensity is set as *k*=15 [9].

Table 5.1 Input values for the bridging law

Matrix Strength		Fc24	Fc30	Fc36	Fc42	Fc48
$P_{max,0} = A \cdot l_b^B$	A	17.02	17.02	17.02	17.02	17.02
	B	0.3354	0.4128	0.4902	0.5676	0.6450
$\delta_{max,0} = C \cdot l_b$	C	0.0327 $(= 0.0218 \times 1.5)$	0.0345 $(= 0.0230 \times 1.5)$	0.0363 $(= 0.0242 \times 1.5)$	0.0381 $(= 0.0254 \times 1.5)$	0.0399 $(= 0.0266 \times 1.5)$
$P_{max} = P_{max,0} \cdot e^{f_p \cdot \theta}$	f_p	0.4586	0.3854	0.3122	0.2390	0.1658
$\delta_{max} = \delta_{max,0} \cdot e^{f_s \cdot \theta}$	f_s	1.6971	1.5195	1.3419	1.1643	0.9867
Fiber strength reduction factor f'		-0.00271				
Fiber strength σ_{fu}, N/mm²		601				
Fiber length l_f,mm		30				
Orientation intensity k		15				

5.4 Calculation Results

The results of bridging law calculation are shown in **Fig. 5.3**. The mark "○" of the curve indicates the maximum tensile stress.

It is apparent from **Fig. 5.3**, the improvement of the matrix strength positively influences the tensile behavior on FRCC. The maximum tensile stress increases almost proportionally as the matrix strength becomes larger.

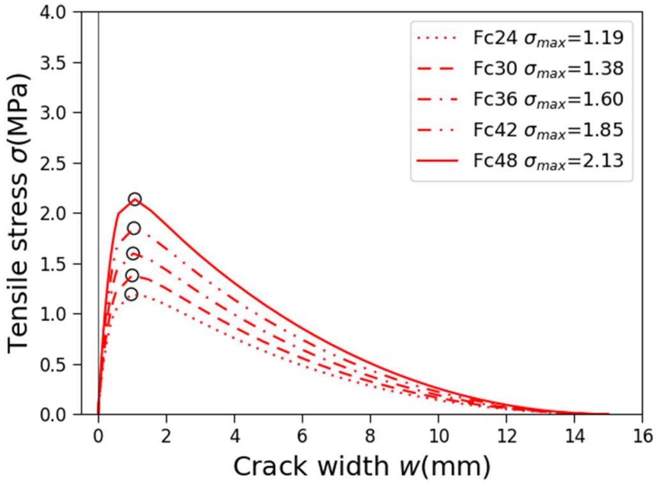

Figure 5.2 Calculation results of the bridging law

Chapter 6 Conclusions

Based on the results of this experiment and the calculation of the bridging law, the following conclusions are drawn:

1. In the pullout test of a single bundled aramid fiber, the fiber was pulled out from the matrix without observing any rupture or peeling of the matrix in most of the test series. In some specimens with a fiber inclined angle of 30°, 45°, 60°, and a long embedded length, clear damage was observed in the embedded area of fibers. A clear rupture in the fibers was also observed under the same conditions.
2. A power function relationship between the maximum pullout load and the embedded length was found. The relationship changes to a nearly linear function with increasing matrix strength. This indicates that the constant bond resistance on the interface is more obvious in the matrix with higher strength. Slip at the maximum pullout load increased as the embedded length became larger, and it is expressed by a linear relationship.
3. The snubbing effect was observed for all test series of the matrix strength. The coefficient of the snubbing effect decreases as the strength of the matrix increases. The same method was applied for the slip at the maximum pullout load, and a similar tendency was observed from the result.
4. The pullout behavior of a single fiber was modeled by the bilinear model based on the results of the pullout test. The bridging law which describes the tensile stress-crack width relationship was calculated based on this model. A group of empirical formulas are proposed based on the test results. The calculation result shows that the improvement of the matrix strength positively influences the tensile behavior on FRCC. The maximum tensile stress increases almost proportionally as the matrix strength becomes larger.

References

[1] Y. Mu; A. Yasojima; T. Kanakubo: Shear Performance of FRCC Beam-Column Joints Using Various Polymer Fibers, Journal of Civil Engineering and Architecture, Volume 13, Number 9, pp.562-571, 2019.9

[2] T. Kanakubo; M. Miyaguchi; K. Asano: Influence of Fiber Orientation on Bridging Performance of Polyvinyl Alcohol Fiber-Reinforced Cementitious Composite", Materials Journal, American Concrete Institute, Vol.113, No.2, pp.131-141, 2016.

[3] Y. Kaneko; M. kunieda; T. Kanakubo; Y. kurihashi: Committee's Report Research Committee of New Application Method on Fiber Reinforced Cementitious Composites, Proceedings of the Japan Concrete Institute, Vol. 34, No.1, 2012.(in Japanese)

[4] Y.W. Chan and V.C. Li: Effects of Transition Zone Densification on Fiber/Cement Paste Bond Strength Improvement, J. Advanced Cement Based Mat., Vol.5, No1, pp.8-17, 1997.

[5] V.C. Li; Y. Wang; S. Backer: Effect of inclining angle, bundling and surface treatment on synthetic fiber pull-out from a cement Matrix, Mater. Res. Soc. Symp. Proc. 114, 159-165, 1988

[6] T. Kanda; V.C. Li: Interface Property and Apparent Strength of High-Strength Hydrophilic Fiber in Cement Matrix. J. Mater. Civ. Eng. 10, 5–13, 1998.

[7] M. Kiyota; H. Mihashi; T. Kanda; A. Kawamata: Study on Bond Characteristics of Fibers in Cementitious Composites. Proc. Jpn. Concr. Inst. 2001, 23, 187–192. (in Japanese)

[8] I. Curosu; M. Liebscher; V. Mechtcherine; C. Bellmann; S. Michel: Tensile behavior of high-strength strain-hardening cement-based composites (HS-SHCC) made with high-performance polyethylene, aramid and PBO fibers, Cement and Concrete Research, Volume 98, Pages 71-81, August 2017.

[9] H. Hashimoto; Y. Mu; H. Yamada; T. Kanakubo: Slip-Out Characteristics of Aramid and PP Fibers and Calculation of Bridging Law, Concrete Research and Technology, Vol.28, pp.103-111, 2017. (in Japanese)

[10] D. Miura; N. Tomoya; T. Kikuta: Study on Pullout Behavior of Single Fiber in FRCC Reinforced by Multiple Fibers, Proceedings of the Japan Concrete Institute, Vol. 42, No.1, 2020. (in Japanese)

[11] Yu-Chen Ou; Mu-Sen Tsai; Kuang-Yen Liu; Kuo-Chun Chang: Compressive Behavior of Steel-Fiber-Reinforced Concrete with a High Reinforcing Index, Journal of Materials in Civil Engineering, Volume 24 Issue 2, February 2012.

[12] T. Kanakubo; S. Echizen; J. Wang; Y. Mu: Pullout Behavior of Bundled Aramid Fiber in Fiber-Reinforced Cementitious Composite", Materials 2020, 13(7), 1746, 2020.

[13] A. Takaku and R. G. C. Arridge: The effect of interfacial radial and shear stress on fibre pull-out in composite materials, Journal of Physics D: Applied Physics, Volume 6, Number 17, 1973

Acknowledgements

I would like to thank all of you for helping me in writing this paper.

My deepest gratitude is first to Professor Toshiyuki Kanakubo, my supervisor, for his constant encouragement and guidance. Without his usual and enlightening guidance, this paper would not have been in its present form.

Secondly, I would like to express my heartfelt thanks to Professor Akira Yasojima and Professor Takashi Matsushima, for their remarkable advises. Thanks also to technical staff Mr. Kojima, without his greatest helping of the preparation, this experiment would not be so successful.

I would also like to thank my dear family for their love and great faith in me for many years. I also want to thank my friends and classmates who have given me help and time to listen to my opinions and help me solve my problems in the difficult process of my paper.

Finally, a sincere gratitude to my great motherland who provided a precious opportunity for me to spend this meaningful three years.